Thermodynamic constraints on fayalite formation on parent bodies of chondrites

Mikhail Yu. ZOLOTOV[1*], Mikhail V. MIRONENKO[2], and Everett L. SHOCK[1, 3]

[1]School of Earth and Space Exploration, Arizona State University, Tempe, Arizona 85287–1404, USA
[2]Vernadsky Institute of Geochemistry and Analytical Chemistry, Russian Academy of Sciences, Kosygin Street 19, Moscow 119991, Russia
[3]Department of Chemistry and Biochemistry, Arizona State University, Tempe, Arizona 85287–1604, USA
[*]Corresponding author. E-mail: zolotov@asu.edu

Abstract–Thermochemical equilibria are calculated in the multicomponent gas-solution-rock system in order to evaluate the formation conditions of fayalite, $(Fe_{0.88-1.0}Mg_{0.12-0})_2SiO_4$, Fa_{88-100}, in unequilibrated chondrites. Effects of temperature, pressure, water/rock ratio, rock composition, and progress of alteration are evaluated. The modeling shows that fayalite can form as a minor secondary and transient phase with and without aqueous solution. Fayalite can form at temperatures below ~350 °C, but only in a narrow range of water/rock ratios that designates a transition between aqueous and metamorphic conditions. Pure fayalite forms at lower temperatures, higher water/rock ratios, and elevated pressures that correspond to higher H_2/H_2O ratios. Lower pressure and water/rock ratios and higher temperatures favor higher Mg content in olivine. In equilibrium assemblages, fayalite usually coexists with troilite, kamacite, magnetite, chromite, Ca-Fe pyroxene, and phyllosilicates. Formation of fayalite can be driven by changes in temperature, pressure, H_2/H_2O, and water/rock ratios. However, in fayalite-bearing ordinary and CV3 carbonaceous chondrites, the mineral could have formed during the aqueous-to-metamorphic transition. Dissolution of amorphous silicates in matrices and/or silica grains, as well as low activities of Mg solutes, favored aqueous precipitation of fayalite. During subsequent metamorphism, fayalite could have formed through the reduction of magnetite and/or dehydration of ferrous serpentine. Further metamorphism should have caused reductive transformation of fayalite to Ca-Fe pyroxene and secondary metal, which is consistent with observations in metamorphosed chondrites. Although bulk compositions of matrices/chondrites have only a minor effect on fayalite stability, specific alteration paths led to different occurrences, quantities, and compositions of fayalite in chondrites.

INTRODUCTION

Although olivine is abundant in meteorites, the ferrous iron-rich end-member, fayalite (Fe_2SiO_4), has only recently been found as a minor secondary mineral in some unequilibrated ordinary and carbonaceous chondrites (Table 1). These rare occurrences of fayalite could indicate unique conditions and/or mechanisms of its formation and may reveal the history of host meteorites. In several unequilibrated ordinary chondrites, fayalite is closely associated with silica-rich chondrules/clasts and forms veins, rims, layers, and lacy networks around them (Brigham et al. 1986; Wood and Holmberg 1994; Wasson and Krot 1994). In these meteorites, fayalite is likely to form through alteration of silica grains. In the Bishunpur (LL3.1) chondrite, fayalite forms rims around kamacite and is in association with troilite (Lauretta et al. 2001; Lauretta and Buseck 2003). In oxidized

CV3 carbonaceous chondrites from the Bali subgroup (Kaba, Mokoia, and Bali), fayalite occurs in the matrix, chondrules, Ca-Al-rich inclusions, dark inclusions, and forsterite-enstatite aggregates (Hua and Buseck 1995; Weisberg and Prinz 1998). In Kaba and Mokoia, fayalite replaces magnetite and coexists with Ca-Fe pyroxene, which sometimes replaces it (Krot et al. 1998a, 1998b, 2004). Fayalite is also present in a Bali-like clasts in the Vigarano CV3 chondrite, where it is associated with magnetite, taenite, sulfides, and Fe,Ni-carbides (Krot and Todd 1998; Krot et al. 2000b; Jogo et al. 2006). In the MacAlpine (MAC) 88107 unequilibrated carbonaceous chondrite, fayalite is found in close association with hedenbergite and magnetite (Krot et al. 2000a).

Mineral assemblages and substitution patterns summarized in Table 1 indicate that fayalite was likely to have formed in asteroidal environments at the expense of primary nebular condensates (kamacite, forsterite, magnesian

Table 1. Summary of the occurrence of fayalite in chondrites.

Chondrite	Fa number	Minerals coexisting with fayalite	Mineral relationships	References
Sharps, H3.4	Fa$_{89-98}$	Silica, low-Ca Px	Rims of Fa around silica grains, silica-bearing chondrules, Fa lace network and veins. Fa is Mn-rich. Fa is secondary to silica. Zonal grains with pure Fa core.	Brigham et al. 1986; Wasson and Krot 1994
Mezö-Madaras, L3.5/6	Fa$_{68-97}$	Silica, Ca-rich Px, Mg-rich Px, merrihueite	Fa veins and crack fillings, Fa rims around silica-bearing chondrules. Silica and merrihueite are replaced by Fa. Zonal grains with pure Fa cores.	Brigham et al. 1986; Wood and Holmberg 1994
ALHA77115, L3.6	Fa$_{71-92}$	Silica, low-Ca Px	Fa rims, layers, and veins in silica clasts. Fa is Mn-rich.	Wasson and Krot 1994
Krymka, L3.1	Fa$_{54-99}$	Silica, low-Ca Px, pentlandite, NiFe oxides, chromite, saponite	Fa rims, layers, and veins in silica clasts. Nonplaty euhedral to subhedral aggregates of Fa in the matrix. Overgrowths of Mn-bearing Fa on forsteritic olivine. Fa as cement.	Wasson and Krot 1994; Weisberg et al. 1997; Weisberg and Prinz 1998
Bishunpur, LL3.1	Fa$_{77-99}$	Troilite, silica, chromite, magnetite, pentlandite, whitlockite, maricite, tetrataenite	Fa and troilite in the matrix and rims on kamacite grains. Fa rims beyond the troilite layers. Lacy patchwork of intergrown Fa and troilite. Fa formed by alteration of kamacite.	Lauretta et al. 2001; Lauretta and Buseck 2003
Kaba, Mokoia, and Bali, CV3$_{oxB}$	Fa$_{88-100}$	Magnetite, hedenbergite, troilite, pentlandite, Ni-rich metal, saponite, minor andradite	Fa in matrix, chondrules, Ca-Al-rich inclusions, dark inclusions, and forsterite-enstatite aggregates and veins. Fa in rims around chondrules, CAIs, and forsterite-enstatite aggregates; around troilite and pentlandite grains; in magnetite-sulfide grains. Parallel Fa and sulfide bands. Sulfides in Fa grains. Fa is Mn-enriched. Fa-magnetite intergrowths. Fa and hedenbergite replace magnetite. Rare Fa replacement by Ca-Fe-rich Px.	Hua and Buseck 1995; Weisberg and Prinz 1998; Hutcheon et al. 1998; Krot et al. 1998a, 1998b, 2004; Choi et al. 2000; Hua et al. 2005
Bali-like clasts in Vigarano, CV3	Fa$_{80-100}$	Magnetite, troilite, Ni-, Co-rich metal, Ni-rich sulfides, Ni-poor sulfides, Fe,Ni-carbides, Ca-Fe Px, phyllosilicates	Fa in opaque nodules in chondrules and in fine-grained rims. Fa-sulfide intergrowth in opaque nodules. Anhedral Fa grains in the matrix. Fa replaces metal and magnetite. Fa-magnetite-troilite veins. Zonal Fa grains with pure Fa core.	Krot and Todd 1998; Krot et al. 2000b; Jogo et al. 2006
Yamato-86009, CV	Fa$_{<100}$	Forsteritic olivine, fayalitic olivine Fa$_{63-71}$, hedenbergite, phyllosilicates; nepheline and sodalite in matrix.	Fa gains in amoeboid olivine aggregates, rare Fa$_{100}$ grains. Zonal Fa grains with Fe-rich core.	Komatsu et al. 2006
MacAlpine (MAC) 88107, ungrouped carbonaceous chondrite	Fa$_{90-100}$	Hedenbergite, magnetite, pentlandite, pyrrhotite	Fa with hedenbergite and magnetite in veins, layers and grains. Fa-hedenbergite intergrowth. Fa overgrows on grains of forsterite and ferrous olivine. Rare Fa-magnetite-Ni-sulfide assemblages. Magnetite replaces metal. Fa replaces magnetite-Ni-sulfide nodules. Fa postdates formation of saponite-serpentine.	Krot et al. 2000a

Fa = fayalite, Px = pyroxene.

pyroxene), products of aqueous alteration on parent bodies (magnetite), or deposited together with secondary minerals (magnetite, Ca-Fe pyroxene, phyllosilicates, Ni-rich metal, chromite, phosphates) that required an aqueous environment (Wasson and Krot 1994; Krot et al. 1998a, 1998b, 2000a, 2004). A parent body formation is supported by ^{53}Mn-^{53}Cr dating of fayalite in Mokoia (7 or 16 Myr after Allende CAIs) (Hutcheon et al. 1998), Kaba (~9.7 Myr after CAIs) (Hua et al. 2005), and MAC 88107 (9 or 18 Myr after CAIs) (Krot et al. 2000a). In an oxidized Bali-like clast in the Vigarano

CV chondrite, the age of fayalite is identical within errors to that in Mokoia and Kaba (Jogo et al. 2006). In Kaba and Mokoia, oxygen isotopic compositions for coexisting fayalite and magnetite indicate parent body incorporation of oxygen from water (Choi et al. 2000; Hua et al. 2005), consistent with the presence of abundant phyllosilicates (Keller and Buseck 1990; Keller et al. 1994). Although parent body formation of fayalite is less evident in unequilibrated ordinary chondrites, it is consistent with the coexistence of fayalite and magnetite, the presence of pentlandite,

phosphates, tetrataenite, and chromite in association with fayalite (observations by Lauretta et al. 2001), and the possible oxidation of kamacite in the presence of aqueous SiO_2, as proposed for CV3 chondrites by Krot et al. (1998b).

Although nebular formation of ferrous olivine is thermodynamically possible below ~600 K, its formation is inhibited by slow Fe diffusion in previously condensed forsterite (Ebel and Grossman 2000; Fedkin and Grossman 2006). Even evaporation of O-rich dusty nebular regions (e.g., Palme and Fegley 1990; Weizberg and Prinz 1998) does not help much to overcome the problem of slow diffusion. This mechanism has not been proposed for the formation of near-pure fayalite and is contradicted by the steep boundaries between fayalite and forsterite, indicating no Fe-Mg interdiffusion on the scale of 3–5 μm (e.g., Krot et al. 2000a). Several other mechanisms of pre-asteroidal fayalite formation (e.g., Hua and Buseck 1995; Lauretta et al. 2001) are less consistent with ages of minerals, oxygen and silicon isotopic data, and mineral substitution patterns (see Krot et al. 2004 and Hua et al. 2005 for recent reviews).

An asteroidal origin of fayalite still remains in debate since specific conditions of formation have not been explored in detail. Thermodynamic analysis of activity (*a*) diagrams in the Fe-Ca-Si-O-H system, with application to CV3 chondrites and MAC 88107 by Krot et al. (1998a, 1998b, 2000a), reveals a possibility of parent body fayalite formation below ~300 °C in the presence of aqueous solution. Here we further explore the stability of fayalite and its formation pathways on parent bodies through thermodynamic calculations. Compared to Krot et al. (1998a, 1998b), who analyzed stability of one-component solids as function of temperature, H_2/H_2O fugacity (*f*) ratio, and activities of solutes, we consider closed multicomponent water-chondrite systems with non-ideal solid, gaseous, and aqueous solutions.

MODEL DESCRIPTIONS

The thermodynamic modeling of aqueous alteration in multicomponent systems has been applied to CM, CI, and CV3 carbonaceous chondrites (e.g., Zolensky et al. 1989; Petaev and Mironenko 1997; Rosenberg et al. 2001; Schulte and Shock 2004). In these works, equilibrium compositions of minerals, aqueous solutions, and gas phases are calculated by the Gibbs free energy minimization method (van Zegeren and Storey 1970). Here we apply this method with the use of the GEOCHEQ code (Mironenko et al. 2000), which was improved by including nonideality of gaseous and solid solutions and to model reaction progress (Mironenko and Zolotov 2005).

The GEOCHEQ code is coupled with a database that contains thermodynamic properties of aqueous species calculated with the revised Helgeson-Kirkham-Flowers (HKF) equations (Tanger and Helgeson 1988; Shock et al. 1992) that incorporate equation-of-state parameters obtained

from analysis of experimental data (Shock et al. 1989, 1997). Properties of gaseous and solid species are mainly from Helgeson et al. (1978) and Holland and Powell (1998). For solid solutions, a subregular mixture model is used to calculate excess free energies of mixing with the Margules mixing parameters listed in Table A1 in the Appendix. Olivine is considered as a binary (fayalite-forsterite) regular solution. Pyroxenes are represented by multiple pseudo-binary solutions with one mixing position (cf. Ottonello 1997). The serpentine, saponite, talc, amphiboles, and a metal alloy are considered as ideal solutions. We calculated activity coefficients of aqueous species in the framework of the Debye-Hückel model. The equation of state after Peng and Robinson (1976) is used to calculate fugacities of the gas species and compressibility of non-ideal gas mixtures. Critical temperature (*T*) and pressure (*P*), Pitzer acentric factors for gases, and binary interactions among H_2, H_2O, CO_2, and CO gases are taken into account. With these data, equilibrium compositions of non-ideal systems can be calculated over a wide range of conditions: 0–500 °C, 1–5000 bar.

With the GEOCHEQ code, equilibria can be calculated in isobaric-isothermal, isochoric-isothermal, or a mixed regime. The isobaric regime could represent conditions when pressure is controlled outside the modeled system. For example, gas escape processes from asteroids (Wilson et al. 1999) or chemical equilibria in hot zones can govern *P* in a porous asteroidal media. In isobaric models, the volume of the system is calculated. The isochoric regime could be typical for warm asteroidal zones that are sealed by recondensed ice. In these conditions, *P* depends on *T*, the volumes of pores and phases present, and the chemical production/consumption of gases.

We modeled progress of alteration reactions in isochoric systems by specifying the amounts of minerals that are allowed to react during each step. At each time step, newly reacted portions of original minerals were allowed to equilibrate with a previously reacted part of the system, which also includes net water. Sequential addition of solids to an original mass of water decreases the local water/rock (*W/R*) ratio in the chemically active part of the system. In isobaric-isothermal systems, chemical evolution of the system as a function of *W/R* ratio can be used as a proxy for alteration progress. In these models, the portion of altered rock (or degree of alteration) corresponds to the ratio of total *W/R* to local *W/R*. In a closed system, completely altered chondrite would be characterized by having the same local *W/R* ratio as the bulk *W/R* ratio before the alteration, regardless of water consumption by the alteration process.

In isochoric-isothermal models, total volume of the system is an input parameter that is calculated from a specified water ice/rock ratio, mineral composition, and the original porosity of the asteroid. Total pressure and the equilibrium composition are computed iteratively. This is
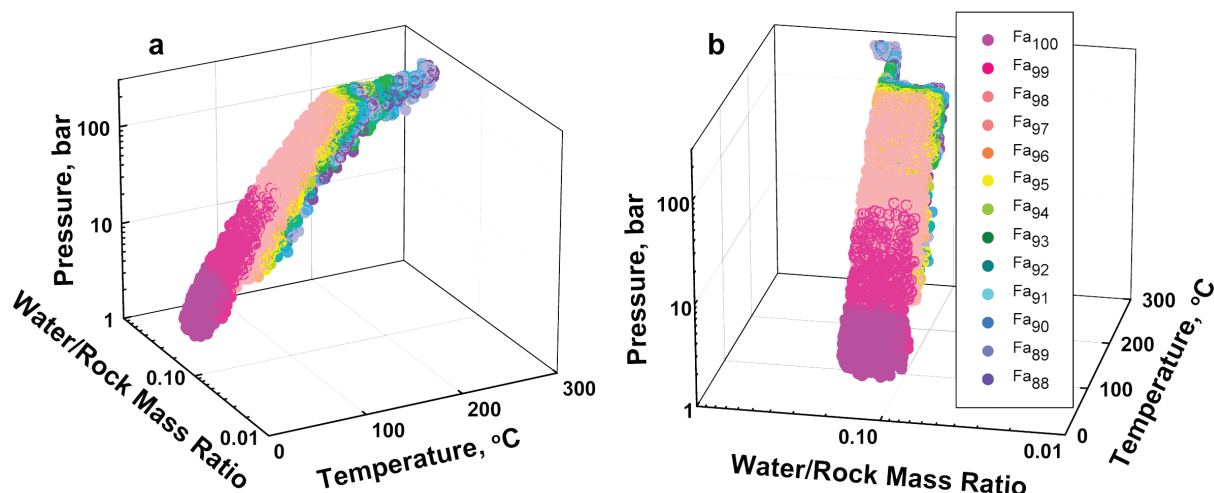
Fig. 1. Conditions of fayalite (Fa$_{88-100}$) formation for the Bali bulk composition. The plotted data are obtained through Monte Carlo calculations of chemical equilibrium in the 17-component water-rock system where T, P, and W/R values are chosen randomly in a course of 10^5 runs. Here and in other figures, the W/R ratio refers to the initial bulk value rather than the ratio in the equilibrium state where H$_2$O has been consumed in reactions. Plots (a) and (b) represent the same results in different projections.

done by a series of equilibrium calculations in isobaric-isothermal systems at various pressures until the calculated volume of the system (gas + solution + solids) becomes equal to the specified volume. Volume of the gas is calculated with the Peng-Robinson equation. Density of aqueous solution is calculated with an equation-of-state for water (Hill 1990) and partial molar volumes of aqueous species computed with the revised HKF model (Tanger and Helgeson 1988).

We model parent body alteration of chondrites through calculations of thermochemical equilibria in the closed system O-H-Mg-Fe-Ca-Si-Al-C-P-S-Cr-Na-K-Cl-Mn-Co-Ni in order to evaluate effects of composition, bulk initial water/rock mass ratio, temperature, total pressure, original porosity and alteration progress on the stability of fayalite. The system includes 123 one-component minerals, 21 mineral solid solutions, a non-ideal gas solution (H$_2$O, H$_2$, CO$_2$, CO, H$_2$S, SO$_2$), and a non-ideal aqueous solution (98 species). Major input data for alteration modeling include masses and elemental/mineral compositions of rock and water (ice, solution), T, total P (in isobaric models), and thermodynamic properties of species. Output results include molar quantities and volumes of each phase, concentrations and activities of gas, aqueous and solid phase components, ionic strength and pH of aqueous solutions, and total volume or pressure (in isochoric models).

We suppressed formation of CH$_4$ due to the inhibition of its formation at low T and P, which is consistent with the presence of carbonates, carbides, and hydrocarbons in unequilibrated chondrites (cf. Brearley and Jones 1998). Bulk compositions of chondrites that contain fayalite, along with other compositions without fayalite, were taken from Jarosewich (1990). Compositions of unaltered H$_2$O-free

chondrites (Table A2) were estimated by decreasing the oxygen abundance so that Fe, Ni, Co, and Cr are present as metal; Mn is present in olivine; and P is present in Fe$_3$P. Hydrogen was introduced to the whole-rock analysis according to the H/C ratio in pyrene (C$_{16}$H$_{10}$) which is used to represent meteoritic organic matter.

RESULTS

The modeling reveals that fayalite (Fa$_{88-100}$) can form below ~350 °C as a minor and rare phase with or without aqueous solution. Stable fayalite is always in equilibrium with H$_2$-dominated gas, and elevated pressures of fayalite formation correspond to elevated partial pressures and fugacities of H$_2$.

Effects of Temperature, Pressure, and Water/Rock Ratio on Fayalite Formation

Fayalite forms at changing temperature and pressure at W/R from ~0.06 to ~0.2. Neither temperature nor pressure significantly affects this narrow range of W/R ratios, as shown in Fig. 1, which depicts T, P, and W/R ratios at which fayalite is present in the equilibrium mineral assemblage calculated for the Bali bulk composition. These results are obtained through a Monte Carlo type of modeling where equilibrium calculations are performed at randomly chosen T-P-W/R conditions. Low-T (<~100 °C) stability of fayalite requires pressures from a few bars to ~80 bar (Figs. 1 and 2). Fayalite formation at higher temperature requires higher pressures. However, possible self-destruction of typical asteroids at internal pressures above ~10^2 bar (Wilson et al. 1999) may restrict high-T formation of the mineral.
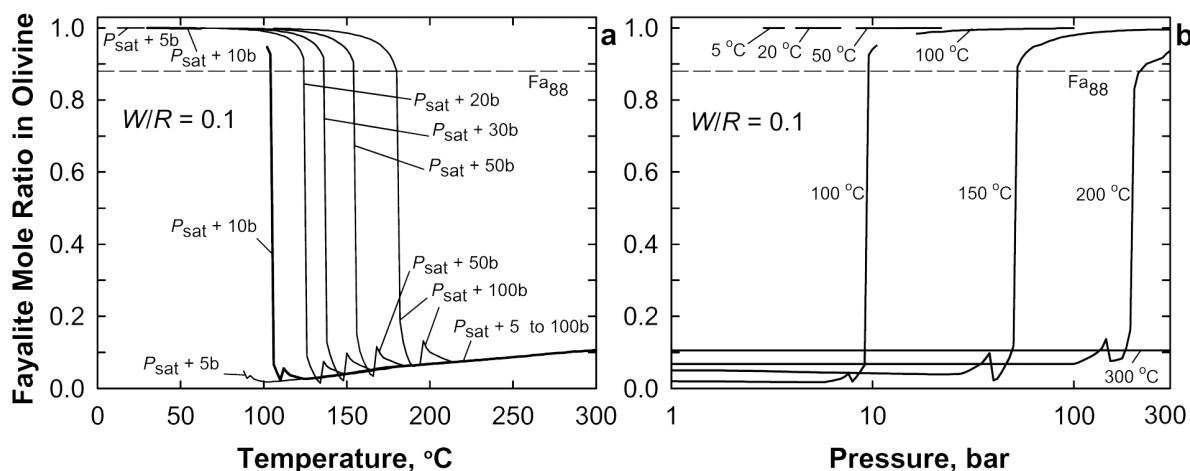
Fig. 2. The composition of olivine as a function of (a) temperature and (b) pressure calculated for the Bali bulk composition at bulk $W/R = 0.1$. In (a), each curve represents a specific pressure above that of water vapor-liquid saturation (P_{sat}). At each temperature, total P is a sum of T-dependent P_{sat} and an indicated pressure value in bars. This additional P term is used to reflect H_2 addition to the system. The horizontal dashed lines show the Fa_{88} composition. The sharp changes in composition of forsteritic olivine in the lower parts of the plots correspond to serpentine-olivine transitions that can also be seen in Fig. 7. An aqueous solution does not exist at these W/R conditions, and at $P < 100$ bar fayalite (Fa_{88-100}) forms only below ~180 °C.

At low temperatures, secondary olivine is present as almost pure fayalite. With increasing temperature, the magnesium content in olivine increases irregularly. The effect of temperature can be seen in Fig. 2a, which shows the equilibrium olivine composition calculated for the Bali composition at a fixed bulk W/R ratio and different P values above T-dependent pressures of water liquid-gas saturation (P_{sat}). The composition ~Fa_{88} represents the most magnesian olivine at the ferrous side of the olivine solid solution. With a very slight increase in temperature, forsterite (Fa_{2-12}) becomes stable. At a single T-P condition, fayalite can coexist with forsteritic olivine, as shown by the vertical lines in Fig. 2. Thermal dehydration of Mg-phyllosilicates causes abrupt compositional changes in forsteritic olivine (to Fa_{5-13}) in the lower parts of Fig. 2 and then Fa content increases gradually as T increases.

At constant temperature, Mg content in fayalite decreases with increasing P (~fH_2), as is illustrated in Fig. 2b. At low P (<~10 bar), fayalite is stable as a low-T pure phase. As pressure increases at T > ~100 °C, forsteritic olivine (Fa_{2-12}) becomes unstable with respect to fayalite (Fa_{88-100}). Further increase in P increases the Fa number until fayalite becomes unstable with respect to Fe-rich metal. At T > ~200 °C, the olivine composition becomes less dependent on P and fayalite does not form at W/R ratios below ~0.15. However, high-T fayalite may form at slightly higher W/R ratios, where aqueous solutions can be stable.

The influence of T and P on the stability and composition of olivine is also shown in Fig. 3 for the Bali composition and a bulk W/R ratio of 0.15. Olivine forms in a broad range of conditions except for low T where Mg-Fe phyllosilicates readily form and high P where Fe-rich alloys are more stable
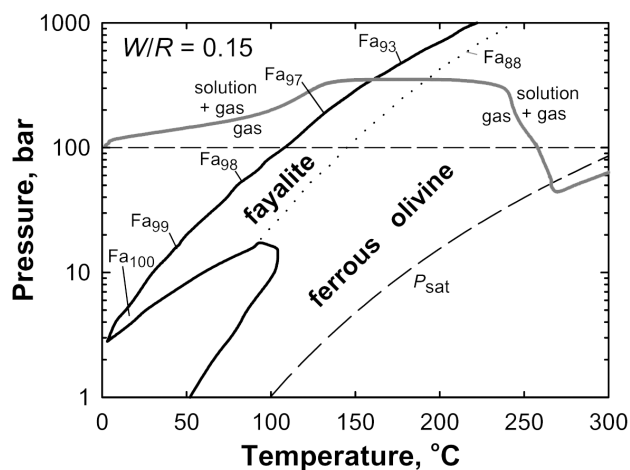

Fig. 3. Stability fields of fayalite (Fa_{88-100}) and ferrous olivine ($Fa_{<88}$) as functions of temperature and total pressure at bulk $W/R = 0.15$ for the Bali bulk composition. The gray curve shows the boundary between aqueous (solution + gas) and metamorphic (gas) conditions obtained through equilibrium calculations. The dashed curve shows the condition of vapor-liquid saturation for H_2O. The horizontal dashed line corresponds to 100 bar pressure at which typical asteroids can be destroyed (Wilson et al. 1999). Fayalite forms in the wedge of P-T conditions that are confined by the dotted curve representing the Fa_{88} composition.

than fayalite. Fayalite is stable in the low-T, high-P part of the olivine stability field. At T < ~50 °C, only pure fayalite forms in a narrow range of P (see also Figs. 1 and 2). At 50–100 °C, forsteritic olivine is stable at low pressures (<~10 bar) and fayalite forms at 10–100 bar. At bulk W/R ratio of 0.15, aqueous formation of fayalite requires pressures that may not represent typical asteroidal values.
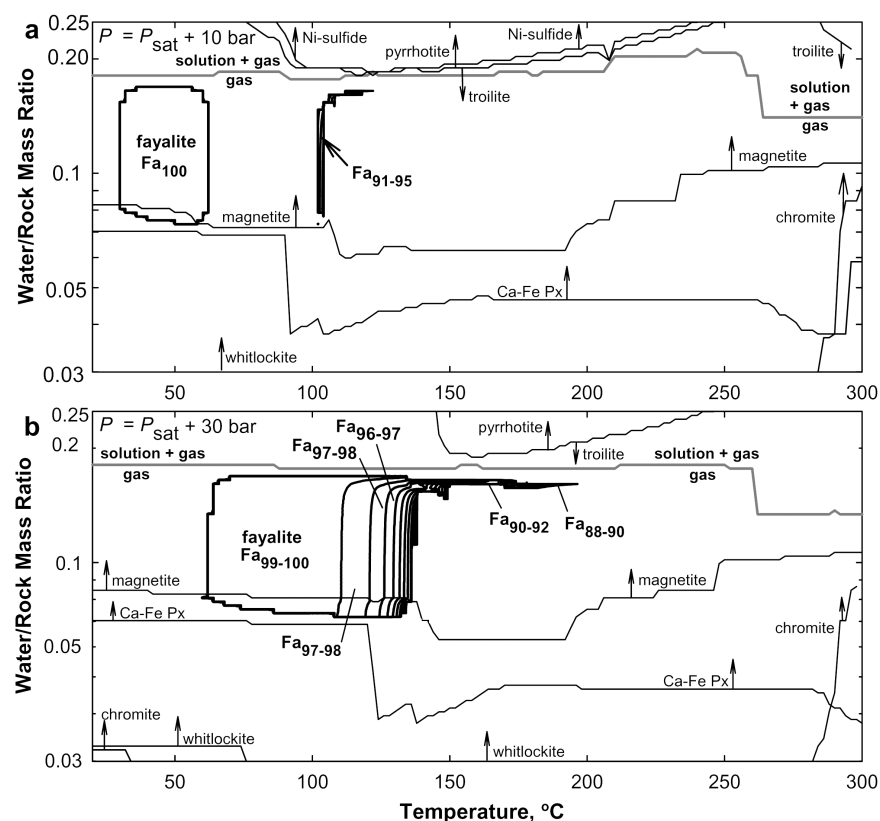
Fig. 4. The fields of fayalite stability and composition as functions of temperature and bulk water/rock ratio. These plots represent equilibrium mineralogy formed through the alteration of the Bali bulk composition at total pressures of (a) 10 bar and (b) 30 bar above P_{sat} at corresponding temperatures. Each plot is developed through calculations of equilibria in the 17-component system in a grid with 4344 cells. The closed fields outlined in black show conditions where fayalite is present in equilibrium assemblages. In each field, the composition of fayalite is indicated. The gray curves show the boundary between aqueous and metamorphic conditions. Other curves with arrows represent boundaries of stability for several minerals present in the equilibrium assemblage. Minerals are present to the side of the curve where each arrow points.

Both temperature and W/R ratio strongly affect the presence of aqueous solution and equilibrium phase associations. Figure 4 shows the stability fields of fayalite, some chondritic minerals, and the boundary between aqueous and metamorphic conditions in coordinates of W/R and T for two P trajectories. An aqueous solution is present at W/R above ~0.13–0.19, depending on T and P. Higher W/R ratios (e.g., the presence of solution) correspond to more oxidizing conditions. As W/R decreases, Ni sulfides, pyrrhotite, magnetite, Ca-Fe pyroxene, whitlockite, and chromite become sequentially less stable. In turn, the stability of these minerals will increase if W/R increases, which may characterize addition of water to extremely reduced nebular minerals.

The W/R ratio has only a minor effect on the composition of fayalite. At low T and/or P, the influence of W/R is negligible (Fig. 4a). At elevated T and P, lower W/R ratios usually correspond to lower Fa numbers. This tendency is illustrated in Fig. 4b, as W/R decreases at ~130 °C. It follows that consumption of water (e.g., solution) would lead to the deposition of sequentially more magnesian fayalite. This effect takes place especially at W/R ratios of ~0.13–0.19,

which also represent the boundary between aqueous and metamorphic conditions. At 150–200 °C, fayalite $Fa_{88–97}$ forms along that boundary (Fig. 4b), and an increase in P further favors fayalite precipitation from solution, as discussed below.

The gas pressure at which fayalite is stable usually exceeds that for saturation with liquid water (Fig. 3). Since H_2 is found to be the dominant component in the gas phase at the conditions of fayalite formation, total P can be considered as a proxy for partial pressure and fugacity of H_2, especially at low-T conditions (Fig. 5). At higher temperatures, increasing deviation of fH_2 from the total P (Fig. 5a) can be accounted for by the presence of H_2O in the gas phase. At the W/R range at which fayalite forms, the fH_2/fH_2O ratio is typically more than unity, while fugacities of other gases are negligible. At a constant W/R ratio below those at which a separate aqueous solution phase forms, the fH_2/fH_2O ratio is almost independent of total P and increases with decreasing T (Fig. 5b), which may also represent low-T hydration of minerals from the gas phase. Elevated fH_2/fH_2O ratios correspond to more reducing conditions and higher Fe^{II} content in olivine at lower temperatures.
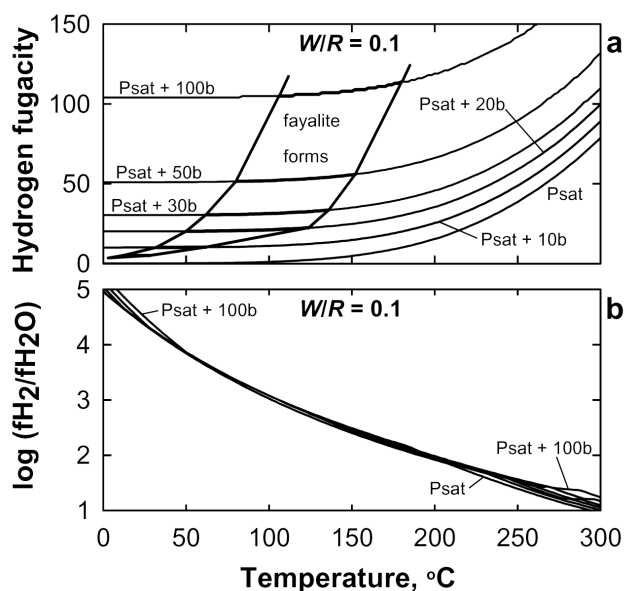
Fig. 5. a) Hydrogen fugacity and (b) the fH_2/fH_2O ratio in the gas phase as a function of temperature and total pressure at bulk $W/R = 0.1$ calculated for the Bali composition. In (a), bold curves mark the boundaries of conditions at which fayalite is present in equilibrium assemblages. Solution does not exist at these conditions, H_2 dominates in the gas phase and total P is mostly determined by the partial pressure of H_2, especially at lower temperature.

Fig. 6. The fH_2/fH_2O ratio as a function of bulk W/R ratio for the equilibrium mineral assemblages that correspond to the Bali bulk composition. Results are presented for two sets of conditions: 50 °C and 10.1 bar (P_{sat} + 10 bar) and 150 °C and 104.8 bar (P_{sat} + 100 bar). The W/R range of fayalite formation at these P-T conditions is shown by the double arrow and dotted lines. Fayalite forms at $\log(fH_2/fH_2O)$ of 2 to 4. The box depicts the boundary between aqueous and metamorphic conditions revealed for the Bali composition. The exact position of that boundary depends on T, P, bulk composition of chondrite, and the list of species included in the calculations.

Fayalite forms only at the specific range of fH_2/fH_2O ratio of about 10^2 to 10^4 (Fig. 6). Lower fH_2/fH_2O ratios characterize aqueous conditions and ferric silicates, such as andradite, can be stable. As W/R decreases at the aqueous to metamorphic transition, the fH_2/fH_2O ratio increases sharply and fayalite can form. Complete reduction of fayalite to Fe metal at lower W/R corresponds to another sharp increase in the fH_2/fH_2O ratio seen at W/R ~0.07 shown in Fig. 6. Higher temperature provides lower fH_2/fH_2O ratios at which fayalite can form (Figs. 5 and 6). The fH_2/fH_2O ratios, total P, and equilibrium compositions of fayalite and other phases at specified conditions are depicted in Tables 2 and 3.

Volumes of fayalite and other secondary minerals in equilibrium assemblages for the Bali composition are depicted in Fig. 7. Low-T mineral assemblages are rich in phyllosilicates (Figs. 7a and 7b). Higher temperature corresponds to lower abundances of hydrated and reduced phases (ferrous olivine, kamacite) and higher abundances of oxidized solids (magnetite). Increases in P in anhydrous systems correspond to more reduced conditions when kamacite becomes abundant and magnetite does not (Figs. 7c and 7d). Changes in W/R (Figs. 7e and 7f) have a dramatic effect on mineral abundances and reflect competitive oxidation (higher T and W/R) and hydration (lower T and higher W/R). Aqueous solutions can exist at lower T, elevated P (Fig. 7c), and $W/R > 0.13–0.18$ (Figs. 7e and 7f). In most of the assemblages, fayalite is a minor secondary phase with
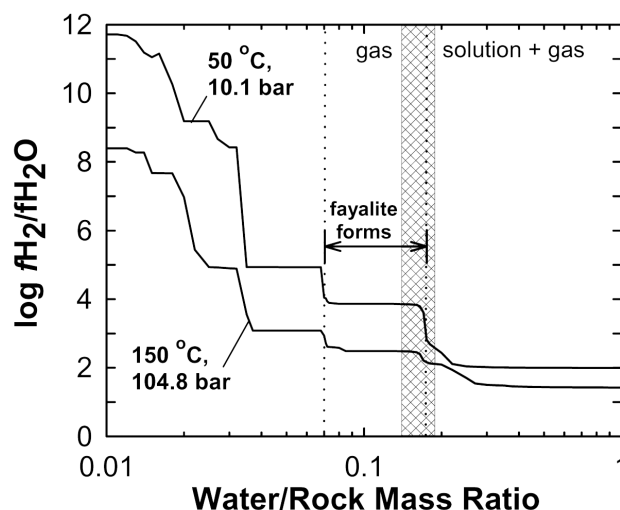
volume typically less than ~3 vol% of completely altered rock. At elevated T and P (Figs. 7b and 7d), the volume of fayalite can reach ~9 vol% (30 cm^3/kg). Incomplete alteration observed in chondritic samples with fayalite implies that these numbers represent upper limits of possible abundance.

Fayalite usually coexists with magnetite (except at low W/R ratios), troilite, phyllosilicates, Ca-Fe-rich pyroxene, phosphates (whithockite), chromite, and condensed organic compounds (Figs. 4 and 7; Table 2). In more reduced environments, which may correspond to lower W/R ratios, lower T, and/or higher fH_2, fayalite also coexists with kamacite. At more oxidizing conditions, fayalite coexists with Ni-, Co-rich metal. At elevated T and P, carbides (cohenite), talc, phlogopite, and amphiboles may also be present in equilibrium assemblages with fayalite (Figs. 7b, 7d, 7f, and Table 2). Under very specific conditions, fayalite can even coexist with forsteritic olivine (Fig. 2).

Fayalite is not present in equilibrium assemblages with some reduced minerals formed through nebular condensation (e.g., forsterite, Mg-rich pyroxene, schreibersite; cf. Ebel 2006). Typically, it does not coexist stably with andradite, pyrrhotite, Ni sulfides, and sulfates that may form at oxidized conditions in the presence of a solution (Figs. 4 and 7). Note however that in silica-rich aqueous systems, fayalite is found in an assemblage with pyrrhotite and Ni sulfide (Table 2, column 8).

Table 2. Examples of equilibrium mineral assemblages with fayalite in parent bodies of chondrites.

	1	2	3	4	5	6	7	8	9	10
T, °C	50	100	150	150	150	150	250	200	150	150
P, bar	10	70	50	50	104.8	104.8	139.7	45.5	104.8	104.8
P above H_2O sat.	10.1	71	45.2	45.2	100	100	100	30	100	100
W/R ratio	0.15	0.15	0.1	0.1	0.1	0.1	0.178	0.1	0.19	0.17
Rock composition	Bali	Bali	Bali	Sharps	Bali	Bishunpur	Bali	Sharps + SiO_2	Bali	Bishunpur
Fayalite	Fa_{100}, 5.0	Fa_{99}, 3.1	Fa_{92}, 26	Fa_{95}, 56	Fa_{99}, 12	Fa_{99}, 40	Fa_{96}, 1.4	Fa_{100}, 63	Fa_{100}, 13	Fa_{100}, 4.7
Ca-Fe pyroxene	30	30	30	17	30	18	30	–	30	–
Serpentine	120	126	105	66	121	102	119	–	213	279
Saponite	82	78	73	114	73	129	86	118	Suppressed	Suppressed
Chlorite	51	52	52	11	52	13	49	–	71	37
Magnetite	44	42	12	17	11	6.8	57	–	32	–
Chromite	1.5	1.5	1.5	1.4	1.5	1.5	1.5	1.0	1.4	1.5
Troilite	9.3	9.3	9.3	13	9.3	14	9.3	–	9.2	14
Fe-Ni-Co metal	5.8	6.3	7.1	14	20	8.1	0.3	0.3	0.4	1.4
Whitlockite	2.0	2.0	2.0	2.1	2.0	2.2	2.0	1.5	2.0	2.2
Halite	0.2	0.2	0.2	0.1	0.2	0.2	–	–	–	–
Pyrene	5.2	5.2	–	8.4	5.2	4.6	5.2	6.1	5.2	4.6
Vol. of minerals	357	357	334	323	340	344	362	340	380	391
H_2 gas	0.999	0.999	0.997	0.996	0.996	0.996	0.908	0.88	0.987	0.988
H_2O gas	1.4×10^{-4}	9.4×10^{-4}	3.5×10^{-3}	3.8×10^{-3}	3.6×10^{-3}	4.1×10^{-3}	9.2×10^{-2}	0.12	1.3×10^{-2}	1.2×10^{-2}
fH_2/fH_2O	7.1×10^4	1.2×10^3	3.0×10^2	2.7×10^2	3.1×10^2	2.7×10^2	11	7.9	88	89
Conditions	Metam.	Metam.	Metam.	Metam.	Metam.	Metam.	Aqueous	Aqueous	Aqueous	Aqueous

The values represent equilibrium mineral compositions formed through alteration of 1 kg of original chondrite (see Table A2). The upper five lines represent input data. For minerals, the data refer to volumes in cm^3. For H_2 and H_2O, the data refer to volume fractions in the gas phase. The fractions of H_2S, CO_2, and CO are below 10^{-4}. "Metam." stands for metamorphic conditions. For case 8, the bulk composition corresponds to Sharps with doubled SiO_2 content. For cases 9 and 10, formation of saponite is suppressed. Serpentine is Mg-rich with Mg/(Fe + Mg) = 0.7–1. Saponite is Mg-rich with Mg/(Fe + Mg) = 0.7–1. Saponite is Na-enriched with Na/(Na + Ca + K) = 0.7–1. Chlorite is Mg-rich (clinochlore) with Mg/(Mg + Fe) = 0.7–1. For cases 7–10, serpentine and chlorite are less magnesian and saponite has less Na. The metal is kamacite (cases 1–3 and 5) and Ni-, Co-rich alloy (other cases). In all compositions, Mn is present as silicates (1–2 cm^3 rhodonite). Compositions 3–7, 9, and 10 contain phlogopite (1–3 cm^3). In case 3, cohenite (12 cm^3) is present. Equilibrium composition 8 also contains quartz (32 cm^3), pyrrhotite (5.6 cm^3), Ni sulfide (3.4 cm^3), ferroactinolite (25 cm^3), and talc (83 cm^3). Composition 10 contains 38 cm^3 tremolite, 4 cm^3 nepheline, and 1 cm^3 sodalite. For cases 7–10, the corresponding solution chemistry is depicted in Table 3.

Alteration Progress at Isochoric-Isothermal Conditions

We modeled progress of alteration reactions in a closed isothermal system at variable bulk W/R ratios and porosities of initial rock-ice mixtures. Changes in solution/gas/mineral composition and pressure are calculated as functions of the portion of reacted rock that characterized alteration progress. The results for 100 °C (Figs. 8 and 9) show that during the stage of aqueous alteration, P increases with reaction progress owing to H_2 production. Early stages of aqueous alteration are characterized by elevated local W/R ratios because inner parts of mineral grains remained unaffected. Further alteration consumed solution via oxidation and hydration reactions and lowered local W/R ratios. Aqueous oxidation causes the formation of chromite, phosphates, magnetite, ferrous silicates, andradite, and Ni-rich sulfides and alloys (Fig. 8). Serpentine and chlorite are the major products of hydration. However, at low bulk water content (typical for fayalite-bearing chondrites), significant parts of the original minerals remained unaltered by the time of solution consumption.

During subsequent metamorphism, unaltered minerals are involved in reactions with alteration products. The progress of metamorphic reactions is characterized by further decreases in the local W/R ratio, as shown in Fig. 8 (right). Early formed minerals (serpentine, chlorite) partially dehydrate producing a new generation of secondary minerals (ferrous olivine, saponite) and water vapor, which is consumed in oxidation. Hydrogen becomes the major species in the gas phase and causes the reduction of minerals (e.g., andradite, magnetite) formed during water-rich stages of alteration. The modeling shows that advanced stages of alteration can lead to the formation of Fe-Mg olivine, Mg-Ca-Fe pyroxenes, feldspars, and secondary kamacite that form through dehydration and reduction reactions. For example, fayalite and kamacite can form at the expense of magnetite at the aqueous to metamorphic transition and at the beginning of the metamorphic stage. Note, however, that the transition from aqueous to metamorphic alteration eventually led to net oxidation of chondrites (McSween and Labotka 1993). Overall, results presented in Fig. 8 illustrate the possibility of isochemical transformation of chondritic mineralogy during the aqueous to metamorphic transition.

Pressure in metamorphic reactions is affected by a complex interplay of redox and dehydration processes that both affect the amount of gas phase and volumes of solid phases. Decreases in the volume of minerals caused by isothermal dehydration, as well as H_2 consumption via reduction, typically cause some decrease in P after consumption of the aqueous solution (Fig. 9). After complete reduction of magnetite at advanced stages of metamorphic reactions (lower part of Fig. 9), some increase in P can be driven by accumulation of H_2. It can be seen that lower initial porosities of rock-ice mixtures correspond to higher P developed along both aqueous and metamorphic alteration paths. Although we calculated many alteration pathways,

Table 3. Activities of components of aqueous solutions for cases 7–10 in Table 2.

	7	8	9	10
NaCl, aq	53	37	2.4	7.0×10^{-2}
Cl^-	7.0	9.1	0.84	2.7×10^{-2}
Na^+	6.2	7.8	15	14
NaOH, aq	6.0×10^{-4}	1.4×10^{-5}	57	46
$NaHSiO_3$, aq	4.6×10^{-5}	1.0×10^{-4}	7.6	28
H_2, aq	8.2×10^{-1}	1.5×10^{-1}	3.6×10^{-1}	3.6×10^{-1}
KCl, aq	1.0	7.3×10^{-1}	8.6×10^{-7}	5.3×10^{-9}
K^+	7.1×10^{-1}	1.2	6.0×10^{-5}	1.2×10^{-5}
KOH, aq	1.1×10^{-4}	3.0×10^{-6}	2.7×10^{-4}	4.7×10^{-5}
$CaCl_2$, aq	7.1×10^{-2}	1.2×10^{-1}	–	–
$CaCl^+$	3.0×10^{-2}	7.4×10^{-2}	–	–
Ca^{2+}	1.4×10^{-4}	1.1×10^{-3}	–	–
$CaOH^+$	5.9×10^{-5}	3.3×10^{-6}	2.4×10^{-9}	–
$MgCl^+$	2.1×10^{-4}	4.7×10^{-3}	–	–
$MgOH^+$	2.7×10^{-6}	1.2×10^{-6}	–	–
Mg^{2+}	6.9×10^{-6}	1.2×10^{-4}	–	–
$MnCl^+$	2.4×10^{-4}	2.3×10^{-2}	–	–
$HMnO_2^-$	–	–	1.9×10^{-4}	3.8×10^{-5}
MnO_2^{2-}	–	–	2.6×10^{-2}	4.7×10^{-3}
MnO, aq	2.8×10^{-7}	1.3×10^{-8}	4.2×10^{-6}	9.5×10^{-7}
Mn^{2+}	9.1×10^{-8}	4.0×10^{-5}	–	–
$FeCl_2$, aq	8.3×10^{-6}	1.1×10^{-4}	–	–
$FeCl^+$	1.3×10^{-6}	3.7×10^{-4}	–	–
FeO, aq	1.0×10^{-6}	9.0×10^{-8}	7.7×10^{-7}	3.7×10^{-7}
$HFeO_2^-$	2.0×10^{-7}	–	2.7×10^{-2}	1.2×10^{-2}
FeO_2^-	3.3×10^{-9}	–	3.8×10^{-5}	1.6×10^{-5}
Fe^{2+}	1.0×10^{-8}	7.9×10^{-6}	–	–
AlO_2^-	2.4×10^{-8}	–	2.0×10^{-4}	2.5×10^{-4}
SiO_2, aq	2.8×10^{-4}	8.2×10^{-3}	5.7×10^{-5}	2.6×10^{-4}
PO_4^{3-}	–	–	8.2×10^{-8}	1.7×10^{-6}
HS^-	6.9×10^{-5}	7.2×10^{-6}	1.3	2.4×10^{-1}
H_2S, aq	5.3×10^{-5}	6.0×10^{-5}	7.5×10^{-7}	1.6×10^{-6}
OH^-	9.3×10^{-5}	3.0×10^{-6}	12	11
CO_2, aq	1.8×10^{-6}	4.9×10^{-7}	–	–
CO_3^{2-}	–	–	3.1×10^{-2}	2.4×10^{-2}
HCO_3^-	1.5×10^{-7}	7.6×10^{-9}	9.2×10^{-5}	8.0×10^{-5}
CH_3OH, aq	3.9×10^{-4}	4.1×10^{-5}	3.5×10^{-5}	3.5×10^{-5}
$COOH^-$, aq	3.5×10^{-6}	6.8×10^{-8}	4.1×10^{-3}	4.1×10^{-3}
H_2O, liq	0.38	0.42	0.30	0.30
pH	6.7	5.4	12.2	12.1
Volume, cm^3	0.1	0.1	2.1	2.4

Activities of solutes below 10^{-10} are not shown. Volume of solution corresponds to 1 kg of rock reacted.

only a few crossed stability fields of fayalite. For example, at 100 °C and initial porosities of 10–50%, fayalite can form at a low bulk W/R ratio of $\sim 10^{-2}$ (Figs. 8 and 9).

Effects of Bulk Chondrite Composition on Fayalite Formation

Equilibrium calculations at variable T-P-W/R conditions performed for various chondritic compositions reveal the same topology of fayalite formation conditions as that obtained for the Bali composition. At specific conditions, fayalite is found to be present in equilibrium assemblages formed in all 10 chondrites considered. Bulk chondritic
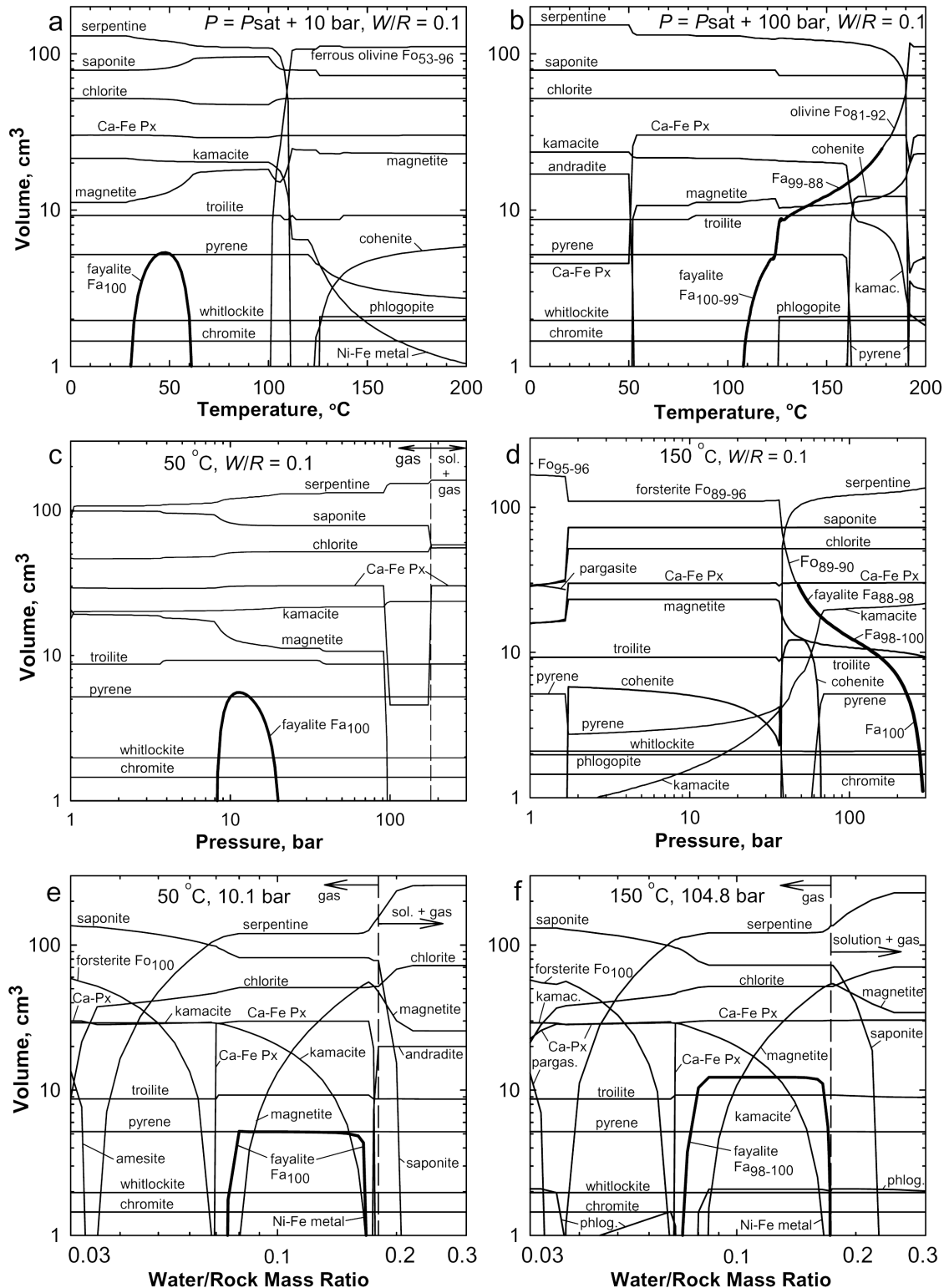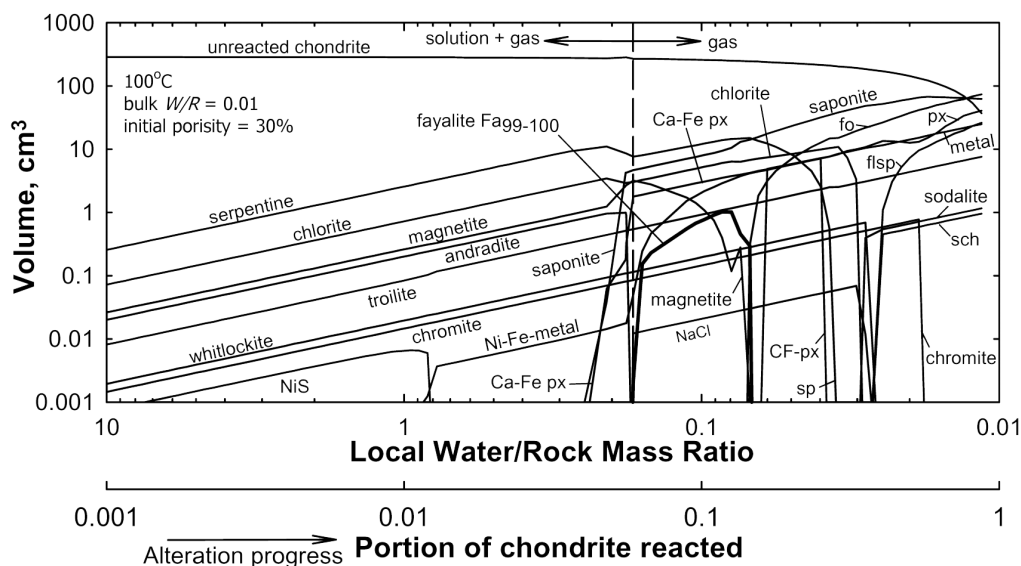
Fig. 7. The volumes of major minerals formed through the alteration of 1 kg of chondrite of the Bali composition as functions of temperature, pressure, and *W/R* ratio. The fixed parameters are shown at the top of each plot. In (a) and (b), pressures are 10 and 100 bar above those of water liquid-gas saturation, respectively. In (e), 10.1 bar = P_{sat} + 10 bar; in (f), 104.8 bar = P_{sat} + 100 bar. The vertical dashed lines show the boundary between aqueous and metamorphic environments. (a), (b), and (d) correspond to metamorphic conditions where no aqueous phase is present. The curves represent changes in volumes of minerals. The fayalite curves are thicker so that they can be easily seen. The composition of fayalite is shown for each curve or for different parts of a curve and can also be seen in Figs. 1–3.

Fig. 8. The volumes of major minerals formed through the isochoric-isothermal alteration of 1 kg of chondrite of the Bali composition at 100 °C, initial (bulk) *W/R* mass ratio of 0.01, and initial porosity of 30%. The local *W/R* ratio shown on the horizontal axis corresponds to the initial *W/R* ratio divided by the portion of chondrite reacted. The vertical dashed line shows the boundary between aqueous and metamorphic conditions. Fo = forsterite; px = Mg-Ca pyroxene; CFpx = Ca-Fe pyroxene; flsp = feldspars; sch = schreibersite; metal = kamacite; sp = serpentine; NiS = millerite; NaCl = halite. Pyrene and Mn silicates are also present in the mineral assemblage. The corresponding changes in pressure can be seen in Fig. 9.

composition has only a limited influence on *T*, *P*, and *W/R* ratio of fayalite formation (Figs. 10a–c). In each case, fayalite forms closest to the boundary between aqueous and metamorphic conditions and is stable predominately along the metamorphic side of the transition (Fig. 10c). Variations in the composition of chondrites seem to influence the amount of fayalite formed (Fig. 10d) rather than its potential appearance. Despite significant differences in the amount of fayalite, chondrites with detected fayalite (Table 1) do not reveal a clear difference in the conditions of fayalite formation. This may imply that changing *T-P-W/R* conditions along alteration paths had more of an influence on fayalite formation than bulk composition.

In an attempt to evaluate the effect of high amounts of silica on fayalite stability, we calculated equilibria with the use of a SiO_2-enriched composition for the Sharps H3 chondrite. The results of this case study show that the addition of SiO_2 expands the temperature field of fayalite formation, makes fayalite more stable in aqueous conditions, and increases its volume fraction in equilibrium assemblages (Fig. 11; column 8 of Table 2). At the bulk composition of Sharps (Si/Fe = 1.25), fayalite forms at temperatures from 40 °C to 140 °C. If silica is added to the Sharps composition, fayalite can form from temperatures below 0 °C to near critical (e.g., at Si/Fe ≈ 2). Fayalite is stable in the presence of aqueous solution above ~160 °C, depending on the composition of the system (Fig. 11). Note that *W/R* ratio and *P* would also affect its stability field (Figs. 4 and 7).

Other calculations show that elevated SiO_2 content in chondrites also expands the range of *W/R* ratios of fayalite
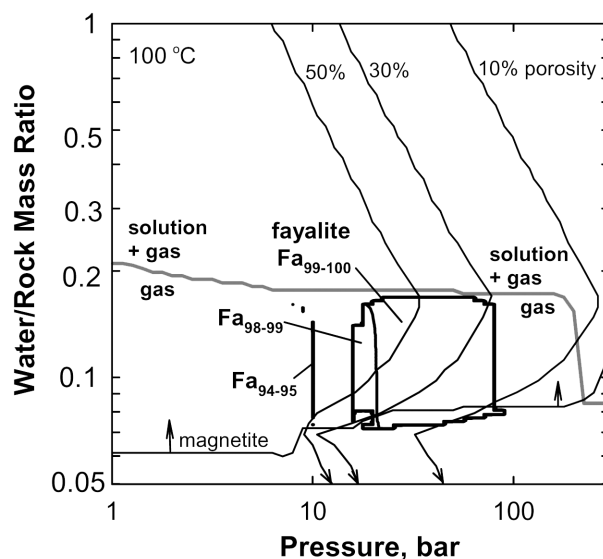

Fig. 9. The fields of fayalite formation as a function of bulk *W/R* ratio and pressure at 100 °C and the Bali bulk composition. The gray curve shows the boundary between aqueous and metamorphic conditions. Curves with arrows represent isothermal alteration pathways at bulk *W/R* ratio of 0.01 and different initial porosities (shown in %). For the pathway with 30% porosity, mineralogical changes are shown in Fig. 8. The small fayalite fields at ~10 bar are real and represent the specifics of chosen conditions.

formation toward lower *W/R* values (Fig. 12). Moreover, an excess of SiO_2 affects the *W/R* conditions of the aqueous-metamorphic boundary and favors aqueous formation of fayalite. Even a small excess of silica can cause aqueous
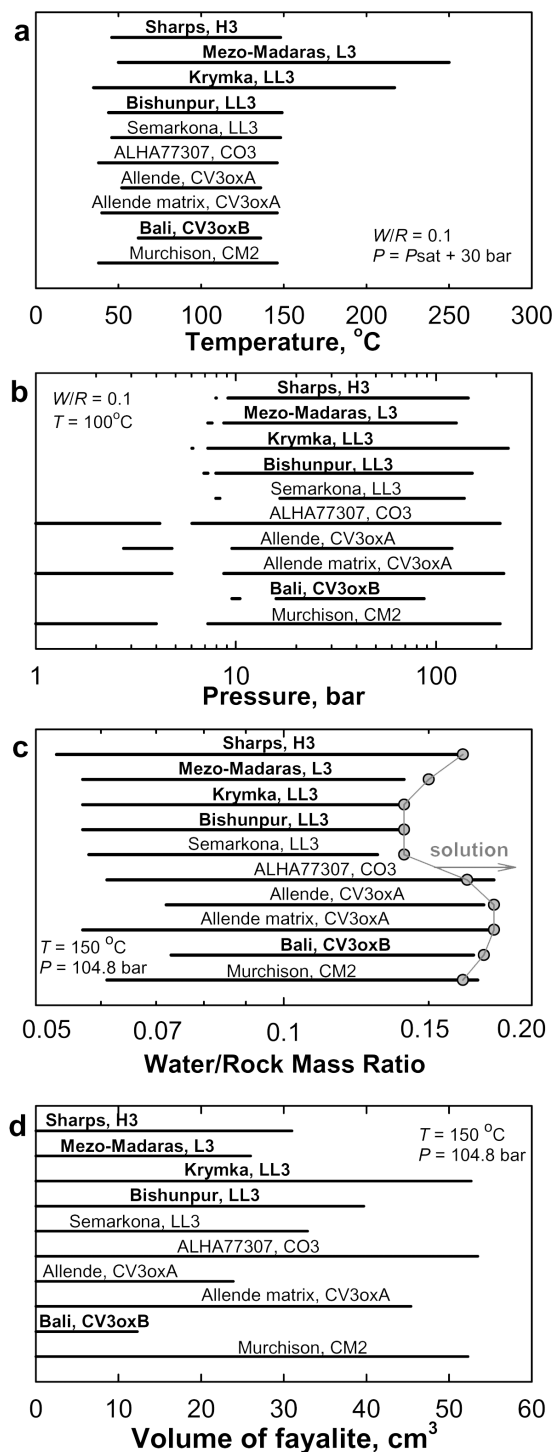
Fig. 10. Conditions of fayalite formation calculated for various chondritic compositions. Names of chondrites with detected fayalite are shown in bold. a) Temperature range of fayalite formation at bulk W/R = 0.1 and pressure 30 bar above that of water-gas saturation. b) Pressure range at which fayalite forms at W/R = 0.1 and 100 °C. c) Water/rock ratio of fayalite formation at 150 °C and 104.8 bar (P_{sat} + 100). The circle symbols show the lower W/R boundary of solution stability. d) Volume of fayalite formed through the alteration of 1 kg of chondrite at 150 °C and 104.8 bar.

deposition of fayalite at the aqueous-metamorphic transition (e.g., before complete consumption of solution). Note that silica phases (here quartz) are typically present in equilibrium associations with fayalite and that the corresponding solution has elevated activity of aqueous (aq) SiO_2 (column 8 in Tables 2 and 3). Although magnetite is typically stable in the presence of solution equilibrated with chondritic compositions (Figs. 4 and 7), it is usually absent from silica-fayalite mineral assemblages, as illustrated in Table 2 (column 8) and observed in Sharps, Mezö-Madaras, ALHA77115, and Krymka.

PATHWAYS OF FAYALITE FORMATION

Since fayalite is stable in a restricted cluster of T-P-W/R conditions, fayalite formation could be caused by changes in any of these parameters. In this section, we analyze our results in an attempt to reveal pathways of fayalite formation as summarized by Reactions 1–10 listed in Table 4 and illustrated by arrows A–F in Fig. 13.

Change in Temperature

At reduced conditions when magnetite is not stable, fayalite can form through oxidation of Fe metal in the presence of silica via Reaction 1 in Table 4. Such a pathway is discussed by Krot et al. (1998b) for asteroidal conditions. Formation of fayalite rather than magnetite is preferable in silica-saturated environments. At slightly more oxidizing conditions, provided by higher W/R, or lower $aSiO_2$(aq) fayalite can form together with magnetite (Reaction 2). Although Reactions 1 and 2 can be driven by a decrease in temperature (arrows A and A1 in Fig. 13), addition of water (arrows B and B1), could have been more important in asteroids. Along with the latter oxidative pathways, fayalite forms first and then magnetite forms together with fayalite.

If temperature decreases, fayalite can also form through the reduction of magnetite by H_2 in the presence of aqueous silica, silica grains, or silicates. Phase diagrams developed by Krot et al. (1998b) and our results show that at the appropriate H_2/H_2O ratio, decreasing temperature in silica-bearing systems could lead to fayalite formation. Reaction 6 involving dissolved silica is a likely pathway (Krot et al. 1998b). Our results also show that other ferrous silicates (e.g., Ca-Fe pyroxene, greenalite) and Fe^0 metal can form through the reduction of magnetite (e.g., Reaction 7). Without silica minerals, the reduction of magnetite can be accompanied by transformations of saponite (Reaction 8; Figs. 7a and 14, arrow A1 in Fig. 13) and ferrous olivine (Fig. 7b; arrow A1 in Fig. 13). The processes can also be driven by a decrease in temperature of aqueous solution (arrow A2). Note that decreasing temperatures at metamorphic conditions can retard both fayalite formation and its transformations through back Reactions 1, 4, and 5 in Table 4.
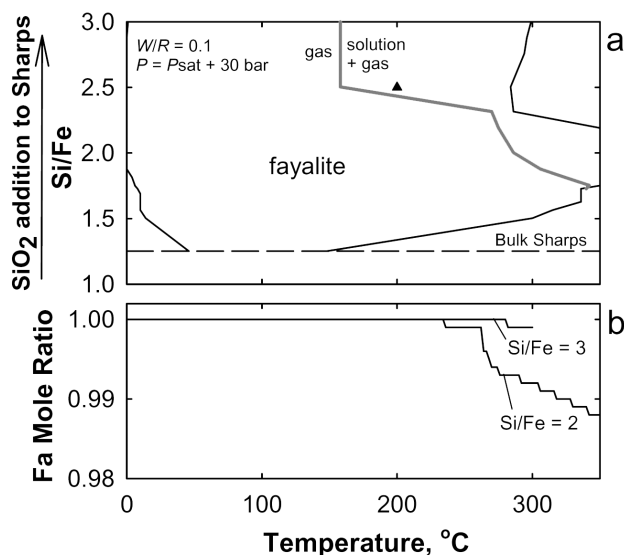
Fig. 11. a) Ranges of fayalite formation and (b) fayalite composition in temperature and Si/Fe ratio corresponding to addition of SiO_2 to the bulk composition of the Sharps H3 chondrite. The results refer to equilibria at $W/R = 0.1$ and pressure 30 bar above that of water vapor-liquid saturation. The horizontal dashed line represents the Si/Fe mole ratio in Sharps. The solid curves indicate the low- and high-temperature boundaries of fayalite formation. The gray curve shows the boundary between metamorphic and aqueous conditions. The triangle corresponds to the conditions depicted in column 8 in Tables 2 and 3. High SiO_2 content expands the temperature of fayalite formation and favors its stability in the presence of solution. Fayalite becomes more magnesian as temperature increases.

Equilibrium calculations for the Bali composition demonstrate that without solid silica, the SiO_2 needed for fayalite formation comes mainly from the oxidation and dehydration of ferrous serpentine (greenalite). In fact, decreases in the abundances of kamacite and serpentine correspond to increases in the amounts of magnetite and fayalite (Fig. 7a). This pathway is represented by Reaction 3 in Table 4 and by arrow C in Fig. 13. Thermal dehydration via Reactions 4 and 5 is possible in reduced anhydrous conditions, when magnetite does not form (arrow C1). Calculation of equilibrium assemblages at $W/R = 0.07$ (Fig. 14) demonstrate fayalite formation through dehydration of phyllosilicates followed by formation of the fayalite-magnetite assemblage at elevated temperatures, consistent with fayalite formation through dehydration of Fe^{II}-serpentine during metamorphism of terrestrial Mg-depleted rocks (Deer et al. 1982). Note that the low-T dehydration of serpentine could be kinetically inhibited, and its high-temperature dehydration produces Mg-rich olivine, not fayalite (Fig. 7b). However in the presence of aqueous solution, increasing temperature increases the solubility, dissolution rates, and corresponding activities of dissolved SiO_2 (e.g., Shock et al. 1989; Dove 1994; column 8 in Tables 2 and 3) all of which facilitates aqueous deposition of fayalite (e.g., pathway C2).
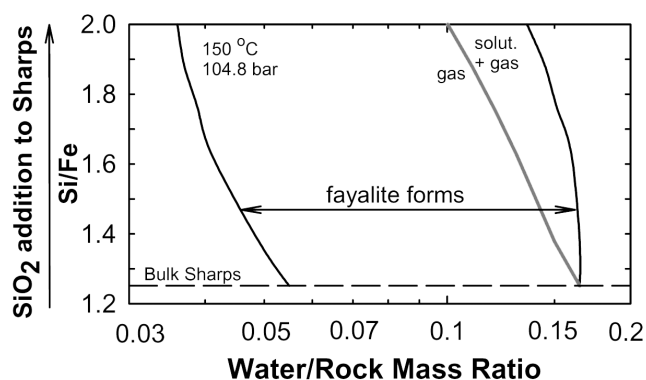
Fig. 12. The effect of adding SiO_2 to the composition of the Sharps H3 chondrite on the W/R range of fayalite formation and on the aqueous-metamorphic boundary at 150 °C and 104.8 bar. The horizontal dashed line represents the Si/Fe mole ratio in Sharps. Addition of silica favors fayalite formation in aqueous conditions. The gray curve shows the boundary between metamorphic and aqueous conditions. Iron-rich fayalite (Fa_{99-100}) forms in the presence of solution, and the composition becomes Mg-enriched at lower W/R.

Since the Fa number decreases with temperature, the non-equilibrium formation of fayalite via pathways C, C1, D, E, and F (Fig. 13; Table 4) can lead to zoned grains where a fayalite core is rimmed by Mg-enriched layers, which is consistent with observations in ordinary (Brigham et al. 1986; Lauretta et al. 2001) and CV3 chondrites (Hua and Buseck 1995; Jogo et al. 2006; Komatsu et al. 2006). Further temperature increase can cause consumption of fayalite through the oxidation to magnetite (at lower T) (Fig. 7a), reduction back to metal (back Reactions 1 and 2, pathway F), or its conversion to ferrous olivine (Fig. 7b, extended pathways C, C1, and D in Fig. 13). The latter conversion is proposed for metamorphosed CV3 chondrites, e.g., Allende (Krot et al. 2004) and can explain the absence of fayalite in type 4–6 chondrites.

Change in Pressure

During asteroidal alteration, pressure is affected by production, consumption, and escape of H_2, as well as changes in volume of pore space and temperature. Oxidation processes cause increases in P because of H_2 generation. The effects of hydration are less clear because consumption of solution and expansion of minerals have opposite effects on the volume of pore space. Low porosities, availability of water, and sealing of outer zones of asteroids all favor pressure increase. Changes in P can be driven by progress of alteration reactions in a local closed area (e.g., Figs. 8 and 9) or by alteration and/or escape of gas in other parts of an asteroid.

Increasing P and the fH_2/fH_2O ratio favors fayalite formation through the reduction of magnetite (Reactions 6–10). If P increases at low T, fayalite, Ca-Fe pyroxene, and ferrous serpentine can form at the expense of

Table 4. Major chemical pathways of fayalite formation in chondrites inferred from equilibrium calculations.

	Reaction	Pathway[a]
Oxidation of iron metal by water		
(1)[b]	$2Fe^0 + 2H_2O(g, liq) + SiO_2(aq, solid) \rightarrow Fe_2SiO_4 + 2H_2(g)$	A, B
(2)	$5Fe^0 + 6H_2O(g, liq) + SiO_2(aq, solid) \rightarrow Fe_2SiO_4 + Fe_3O_4 + 6H_2(g, aq)$	A1, B1
(3)	$4Fe^0 + 3H_2O(g, liq) + Fe_3Si_2O_5(OH)_4 \text{ (in serpentine)} \rightarrow 2Fe_2SiO_4 + Fe_3O_4 + 5H_2(g, aq)$	C
(4)	$Fe^0 + Fe_3Si_2O_5(OH)_4 \text{ (in serpentine)} \rightarrow 2Fe_2SiO_4 + H_2O(l, g) + H_2(aq, g)$	C1
Dehydration of ferrous serpentine (greenalite)		
(5)	$2Fe_3Si_2O_5(OH)_4 \text{ (in serpentine)} \rightarrow 3Fe_2SiO_4 + SiO_2(aq, solid) + 4H_2O(l, g)$	C1
Reduction of magnetite by hydrogen		
(6)[b]	$Fe_3O_4 + 1.5SiO_2 \text{ (aq, solid)} + H_2(g, aq) \rightarrow 1.5Fe_2SiO_4 + H_2O(gas, liq)$	A1, E, F
(7)	$Fe_3O_4 + SiO_2(aq, solid) + 2H_2(g, aq) \rightarrow Fe_2SiO_4 + Fe^0 + 2H_2O(gas, liq)$	A1, E, F
(8)	$Fe_3O_4 + 1.5SiO_2 \text{ (from saponite)} + H_2(g, aq) \rightarrow 1.5Fe_2SiO_4 + H_2O(gas, liq)$	A1, E, F
(9)	$Fe_3O_4 + Fe_3Si_2O_5(OH)_4 \text{ (in serpentine)} + SiO_2 \text{ (aq, solid)} + H_2(g, aq) \rightarrow 3Fe_2SiO_4 + 3H_2O(gas, liq)$	E, F
(10)	$Fe_3O_4 + Fe_3Si_2O_5(OH)_4 \text{ (in serpentine)} + 3H_2(g, aq) \rightarrow 2Fe_2SiO_4 + 2Fe^0 + 5H_2O(gas, liq)$	E, F

[a] The example pathways are shown by the gray arrows in Fig. 13. Some pathways can also be seen in Fig. 7.
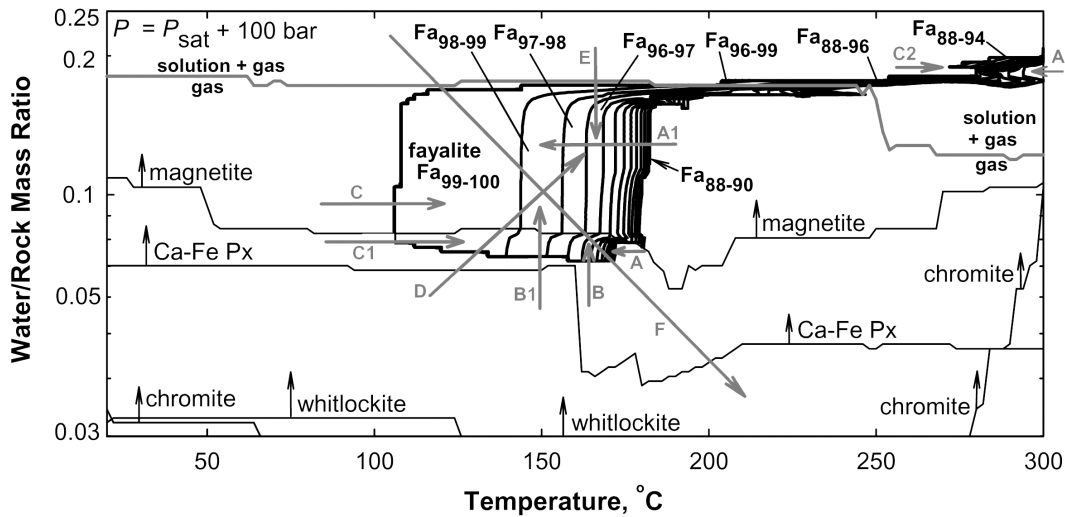[b] Reaction considered by Krot et al. (1998a, 1998b).

Fig. 13. The field of fayalite stability and fayalite composition as functions of temperature and initial *W/R* ratio at total pressures that are 100 bar above P_{sat}. The plot represents equilibrium mineralogy formed through the alteration of the Bali bulk composition (see capture for Fig. 4 for details). The gray arrows illustrate possible pathways of fayalite formation as described in the text. The relationships between pathways and chemical reactions are outlined in Table 4.

magnetite and silica released from a silicate (e.g., saponite, Fig. 7c). At higher *T*, fayalite forms as a part of an olivine solid solution along with a secondary Fe-rich metal and ferrous serpentine (Fig. 7d). Since the Fa number increases with *P* (Figs. 2 and 9), olivine grains could be rimmed by fayalite. Further increase in *P* may cause the reduction of fayalite and magnetite to secondary kamacite (back Reactions 2 and 3). Without magnetite, fayalite is reduced via back Reactions 1 or 4. Pressure variations during metamorphic transformations could also have affected fayalite stability (Fig. 9). Decreasing *P*, due, for example, to decompression of outer asteroidal regions, creates more oxidizing conditions at which fayalite and magnetite can be products of Fe^0 metal oxidation (Reactions 1 and 2), and magnesian rims could be formed around fayalite grains.

Change in Water/Rock Ratio

Fayalite can form as *W/R* increases (oxidative pathway) and decreases (reductive pathway), as can be seen in Figs. 7e and 7f. The oxidative pathway yields the sequential formation of secondary minerals through oxidation by water vapor: chromite, whitlockite, ferrous serpentine, fayalite (arrow B in Fig. 13), and then magnetite (arrow B1). Fayalite is predicted to form through oxidation of kamacite in the presence of silica or silicate minerals (Reactions 1–3). If formed at higher temperatures, fayalite grains could have a magnesian core rimmed by pure fayalite (a continuation of paths B, B1). This process could have been facilitated by heating (path D) that increased diffusion rates and could be favored by dehydration of ferrous serpentine (Reactions 3

and 4). If so, an aqueous solution is not needed and further oxidation by H_2O vapor can cause transformation of fayalite to other minerals (magnetite).

Decreases in local W/R ratio can cause formation of fayalite through reductive pathways (Figs. 6, 7e, and 7f, arrows E and F in Fig. 13). During the transformation from aqueous to metamorphic alteration, decreasing local W/R ratios can reflect increases in the amount of chondrite reacted (Figs. 8 and 9). Progress of reactions that consume H_2O leads to increases in the fH_2/fH_2O ratio and total P, making the gas and aqueous phases more reduced. Close to the aqueous-metamorphic boundary, an increase in the fH_2/fH_2O ratio facilitates the reduction of magnetite to fayalite by Reactions 6–8. The possibility of fayalite formation in association with secondary Fe^0-rich metal (Reactions 7 and 10) can be inferred from equilibrium models (Figs. 7e, 7f, and 8). With or without an excess of silica, formation of fayalite can be facilitated by the dehydration of ferrous serpentine (Reactions 9 and 10).

If kinetics allow, further progress of reductive metamorphic reactions could transform fayalite to Fe^0 metal, while released silica may contribute to the formation of saponite (Figs. 7e, 7f, and 8). This process could be followed by the reduction of Fe^{II} in Ca-Fe pyroxene, which remains stable at higher degrees of alteration at lower W/R ratios and at higher temperatures compared to fayalite. Although these metamorphic transformations could occur in an isothermal regime (pathway E), typical alteration progress was likely to be accompanied by changes in P and an increase in T (pathway F).

Observation of zoned fayalite grains with more magnesian rims (e.g., Hua and Buseck 1995; Jogo et al. 2006; Komatsu et al. 2006) implies that fayalite formation could have been accompanied by decreasing W/R ratios and/or increasing T (Figs. 4b and 13, pathways E and F). In addition, a possibility exists that Mg-rich rims form during an increase in both W/R and T (pathway D). Formation of zoned fayalite can occur only at elevated T and P and implies geologically rapid changes in T-P-W/R conditions to prevent reequilibration within olivine grains.

Aqueous versus Metamorphic Formation of Chondritic Fayalite

Although a metamorphic origin for fayalite looks more favorable in thermodynamic models, aqueous deposition is also possible and consistent with observations. Elevated T, P, and aSiO$_2$(aq) all favor fayalite formation in the presence of solution. Higher solubilities of chondritic silica species relative to quartz also contribute to elevated aSiO$_2$(aq) and to an expansion of the temperature stability of fayalite. At acidic pH, high activities of silica can account for intensive dissolution of amorphous phases in matrices and silicates. In strongly alkaline solutions, typical for chondritic
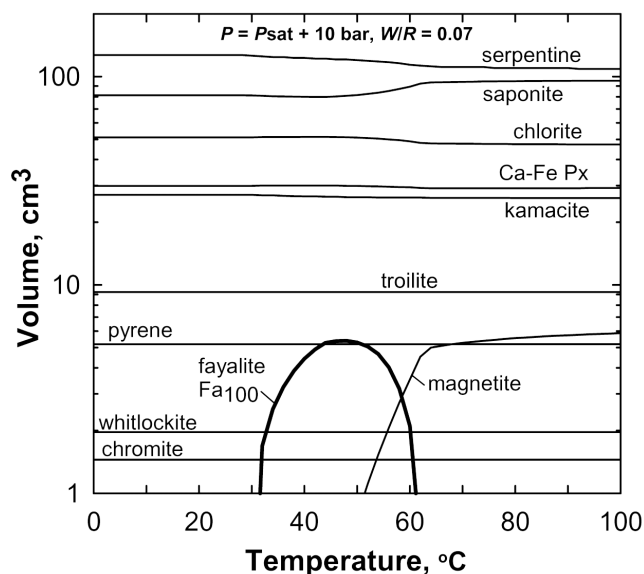

Fig. 14. The volumes of major secondary minerals representing Bali bulk composition at W/R ratio of 0.07 as functions of temperature. The results represent equilibrium mineral assemblages at pressures 10 bar above that of water vapor-liquid saturation. Aqueous solution is not present at these conditions. If temperature increases, fayalite can form through dehydration of ferrous serpentine. If temperature decreases, magnetite can be reduced by H_2 to fayalite and other ferrous silicates.

environments (Zolensky et al. 1989; Rosenberg et al. 2001) elevated aSiO$_2$(aq) can be caused by elevated solubility of silica grains, especially amorphous silica phases. Elevated T, pH, high activities of Na and Cl species, and dissolution of amorphous silica should have led to high rates of silica dissolution (Dove 1994; Icenhower and Dove 2000). In all cases, the presence of silica grains further increases aSiO$_2$(aq) (up to ~0.04 in our models), which expands the stability field of fayalite into the field of solution (Figs. 11 and 12; Tables 2 and 3).

Equilibrium models also show that low activities of Mg solutes favor aqueous formation of fayalite, consistent with the occurrence of fayalite in terrestrial Mg-depleted hydrothermal deposits. Although the presence of Mg-rich phyllosilicates in secondary assemblages accounts for low activities of Mg solutes, the activities are even lower if saponite is not present (columns 9 and 10 in Tables 2 and 3). In typical aqueous to metamorphic alteration pathways (Figs. 7e, 7f, and 8), thermodynamically favored serpentine to saponite conversions could have been inhibited owing to the extremely slow dissolution of serpentine in non-acidic environments (Bales and Morgan 1985). Suppression of saponite formation expands the conditions of fayalite stability into the field of solution, as can be seen when Figs. 7e and 7f are compared with saponite-free models in Fig. 15. At low T and P, fayalite can precipitate from solution right at the aqueous to metamorphic transition in association with
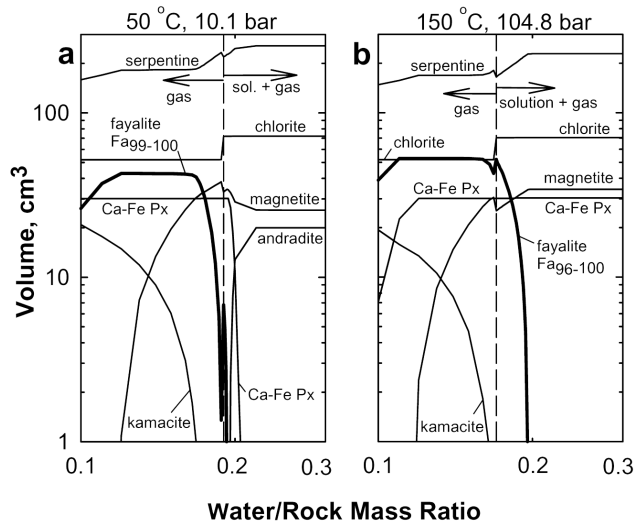
Fig. 15. The volumes of several major minerals in equilibrium mineral assemblages if saponite formation is suppressed at the Bali bulk composition. The calculations are performed at the same *P-T* conditions as in Figs. 7e and 7f. Inefficient isothermal dehydration of serpentine may account for inhibition of saponite formation. Without saponite, fayalite readily forms in aqueous conditions, especially at higher temperatures (compare to Figs. 7e and 7f).

Fig. 16. The range of *W/R* ratios at which fayalite can form in various chondrites at 150 °C and 104.8 bar (P_{sat} + 100 bar) if formation of saponite does not occur. The circle symbols show the calculated lower *W/R* boundary of solution stability for each composition. Comparison with Fig. 10c shows that inhibition of saponite formation expands the conditions of fayalite stability into the field of aqueous solution.

magnetite, chlorite, serpentine and Ca-Fe pyroxene (Fig. 15a). At elevated *T* and *P*, the same mineral assemblage can precipitate in water-rich aqueous conditions (Fig. 15b). A decrease in the *W/R* ratio from ~0.2 (water consumption) can cause fayalite deposition at the expense of magnetite and serpentine. Figure 15 also demonstrates formation of larger amounts of fayalite compared to saponite-bearing cases.

Saponite-free models developed for several chondritic compositions emphasize the possibility of aqueous deposition of fayalite (Fig. 16). For all compositions considered, control of Mg solutes by serpentine and chlorite can cause fayalite formation before consumption of solution.

Our models show that fayalite coexists with concentrated aqueous solutions that are characterized by low activity of water and high activity (~0.1) of dissolved H_2. Depending on conditions, the major solutes are $NaCl(aq)$, Na^+, Cl^-, $NaOH(aq)$, $NaHSiO_3(aq)$, K^+, $H_2(aq)$, OH^-, and HS^- (Table 3). The activity of $SiO_2(aq)$ is in the range of 5×10^{-5} to $~10^{-2}$. The activities of Fe^{II}-solutes (mostly $HFeO_2^-$ and chloride complexes) are at or below the 10^{-2} level. The pH varies from slightly acidic values in Cl-rich concentrated solutions to strongly alkaline values.

Earlier calculations by Michael Petaev (unpublished, private communication) and our models show elevated activities of Mn^{II} species (10^{-2}–10^{-3}) in aqueous solutions that coexist with fayalite. It follows that hydrothermally deposited fayalite could be enriched in Mn. In fact, the high abundance of Mn in fayalite from ordinary chondrites and CV3 chondrites (up to ~1.5 wt%) has been used as an argument for parent body formation when Mn is supplied
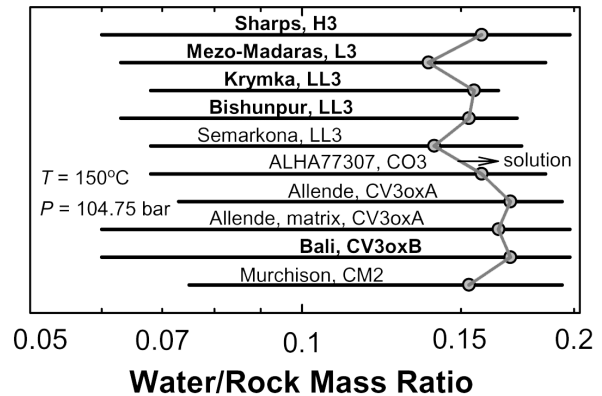
from early altered matrices (Wasson and Krot 1994; Krot et al. 2004). Variations in Mn/Fe ratios in ferrous olivine in ordinary and CV3 chondrites (Hua and Buseck 1995; Weisberg et al. 1997; Weisberg and Prinz 1998) do not contradict this interpretation.

In Earth's hydrothermal systems, fayalite is a rare mineral that forms in $Fe^{(II)}$-, SiO_2-rich environments with low concentrations of Mg solutes (e.g., Rasmussen et al. 1998). The common use of the quartz-fayalite-magnetite (QFM) buffer in hydrothermal experiments (Kishima and Sakai 1984) indicates the lack of strong kinetic constraints for silica-fayalite-magnetite conversions. Without aqueous solution, low-*T* formation of fayalite is limited by diffusion rates. It appears that the transition from aqueous to metamorphic behavior marks a "stalling point" in kinetics of these systems. Note however, that thermal dehydration of phyllosilicates (e.g., serpentine, Fig. 8) at that transition could have supplied solution (Krot et al. 2004) and silica that extended the duration of fluid-assisted deposition of fayalite.

Despite the likely aqueous deposition of some chondritic fayalite, a metamorphic origin is also possible. Solid state reequilibration of aqueously formed secondary phases and primary minerals could have led to fayalite if *T-P-f*H_2/*f*H_2O conditions overlapped with its stability field. In some cases, fayalite grains deposited from aqueous solution can continue to grow after solution has been consumed. As an example, reduction of magnetite and release of silica from dehydrated phyllosilicates could be the major reactions leading to small fayalite grains in rims in matrix (Reactions 3–5, 8–10). In fact, dehydration of phyllosilicates has been proposed as a major formation mechanism for ferrous olivine in CV3 chondrites (Kojima and Tomeoka 1995; Krot et al. 1997). The lack of mass-dependant fractionation of oxygen isotopes in

CV3 chondrites (Clayton and Mayeda 1999) may indicate lower bulk *W/R* ratios compared to metamorphosed CI and CM chondrites rather than an inconsistency with dehydration of phyllosilicates. Thermal metamorphism of phyllosilicates and magnetite in veins deposited from earlier aqueous conditions can lead to veins containing fayalite.

Origin of Fayalite in Ordinary and Carbonaceous Chondrites

Fayalite-silica aggregates, veins, and crack fillings in silica-bearing chondrites, Sharps, Mezö-Madaras, ALHA77115, and Krymka (Brigham et al. 1986; Wasson and Krot 1994; Wood and Holmberg 1994) may reveal aqueous deposition, consistent with our models for SiO_2-enriched compositions (Figs. 11 and 12; column 8 in Tables 2 and 3). The presence of merrihueite, $(K,Na)_2Fe_5Si_{12}O_{30}$, (in Mezö-Madaras, Dodd et al. 1966; Wood and Holmberg 1994) in fayalite-silica assemblages may be indicative of alkali-rich aqueous solutions (Krot and Wasson 1994). In Krymka, the observed pentlandite-fayalite relationships (Weisberg et al. 1997) are consistent with evolution of an oxidized fluid (when pentlandite and NiFe oxide formed) toward H_2-rich conditions at which Mn-bearing fayalite formed. Observation of fayalite as a cement material (Wasson and Krot 1994) is consistent with its deposition during late stages of aqueous alteration. Decreasing Fe/Mg ratios toward rims of a fayalite-bearing fragment in Sharps (Brigham et al. 1986) may indicate an increase of temperature, which also could have occurred during metamorphism. Temperatures of fayalite formation in SiO_2-saturated aqueous system can vary from ~150 °C to the critical temperature of water (Fig. 11). Higher temperatures can also be possible but were not considered here.

Although the origin of silica grains is not known, silica and fayalite could have formed in a single process. First, aqueous fluids liberated silica from amorphous silicate material in matrix and oxidized kamacite. Subsequent consumption of solution in oxidation reactions caused H_2 production and deposition of silica, followed by the formation of fayalite from SiO_2-saturated H_2-rich fluids. This is consistent with the formation of fayalite after silica grains observed in chondrites.

The formation mechanism of fayalite-bearing matrix and rims on kamacite grains in the Bishunpur LL3.1 is less certain. Although Lauretta et al. (2001) and Lauretta and Buseck (2003) do not report signs of aqueous processes in fayalite-bearing associations and suggest nebular formation, the described association of fayalite with magnetite, troilite, chromite, and whitlockite, as well as the presence of silica grains, are consistent with parent-body formation. On the one hand, formation of fayalite can be explained by reactions in which kamacite and Si^o were oxidized by water vapor. On the other hand, the presence of pentlandite and Ni-rich metal in

fayalite-bearing rims may indicate an oxidized, possibly aqueous, early stage of alteration at locally high *W/R* ratios and a low fH_2/fH_2O ratio. In fact, maricite $(NaFePO_4)$ present in rims and in the matrix (e.g., Lauretta et al. 2001) could be a sign of an aqueous environment in which Na was mobile. Minor aqueous alteration in Bishinpur is consistent with the presence of amorphous material of feldspathic composition and a Cl-bearing smectite clay (Alexander et al. 1989). Fayalite may have been deposited at the aqueous to metamorphic transition, consistent with a decrease in the Fe/Mg ratio in fayalite with distance from the metal surface (Lauretta et al. 2001). Subsequent mild metamorphism (Rambaldi and Wasson 1981) might have contributed to additional growth of Mg-bearing fayalite grains, but did not cause their transformation to other minerals.

The mineralogy of oxidized CV3 fayalite-bearing chondrites from the Bali subgroup, in Yamato-86009, and in MAC 88107 (Keller and Buseck 1990; Keller et al. 1994; Krot et al. 1998a, 1998b, 2000a, 2000b, 2004; Hua and Buseck 1995; Jogo et al. 2006; Komatsu et al. 2006) is also consistent with an aqueous to metamorphic alteration scenario. This is supported by 1) observed formation of fayalite after serpentine and saponite, 2) occurrence of fayalite around pentlandite-bearing clusters, 3) replacement of magnetite-Ni-sulfide nodules by fayalite, 4) replacement of fayalite by Ca-Fe pyroxene, and 5) formation of zonal fayalite grains with Fe^{II}-rich core. Fayalite grains were probably formed at H_2-rich conditions shortly before consumption of solution and had the potential to grow during the subsequent metamorphic stage. The decrease in size of fayalite grains with the decrease in Fa number (Hua and Buseck 1995) may reveal slowing rates of fayalite formation at the aqueous-metamorphic transition. Elevated concentration of Mn in fayalite is consistent with aqueous deposition (e.g., Krot et al. 2000a, 2004). Model results showing formation of fayalite in association with Ca-Fe pyroxene, magnetite, and troilite are consistent with these observations. According to our models, the observed replacement of magnetite by fayalite could also have occurred at the metamorphic stage. In particular, magnetite in hydrothermally-formed veins could have been replaced by fayalite. Rare fayalite replacement by Ca-Fe-rich pyroxene (Krot et al. 1998b) indicates the beginning of an advanced stage of metamorphic transformations that would have been characterized by lower local *W/R* ratios, higher fH_2/fH_2O ratios and higher temperature. In Yamato-86009 CV chondrite, rarity of Fa_{100} grains (Komatsu et al. 2006) could be accounted for high-*T* transformation of early formed faylite, consisted with the presence of nepheline, sodalite, and lath-shaped fayalitic olivine in matrix. However, further metamorphic transformations of fayalite may have been terminated through destruction of the parent body. The general pathway of mineral transformation during this aqueous to metamorphic scenario is illustrated by Fig. 8 and arrow F in Fig. 13. Note that metamorphic alteration in the

CV$_{oxA}$ group (e.g., Allende, ALH 84128) proceeded further and ceased at higher *T* and lower *W/R* ratios compared to meteorites from the CV$_{oxB}$ group (Kaba, Bali). This is consistent with observed enrichment in Mg in ferrous olivine by comparing Kaba to Allende, in which fayalite could have been replaced by more magnesian olivine (e.g., Krot et al. 2004). In Allende, thermal metamorphism could have led not only to dehydration of phyllosilicates (Kojima and Tomeoka 1996; Krot et al. 1995; Brearley 1999) but also to reduction of magnetite.

The proposed scenario of fayalite formation below ~350 °C generally agrees with interpretations of isotopic data that revel higher $\delta^{18}O$ values in fayalite than in coexisting magnetite (Hutcheon et al. 1998; Choi et al. 2000). The scenario is also consistent with chemical compositions of minerals and phase relationships observed in oxidized CV3 chondrites with different degree of metamorphism (e.g., Kojima and Tomeoka 1996; Krot 1998a, 1998b, 2004) and in MAC 88107 (Krot et al. 2000a). In addition, our considerations of fayalite stability are in general agreement with argumentation and analysis of activity diagrams by Krot et al. (1998a, 1998b). However, their analysis was partially based on diagrams in which an aqueous solution was not considered (Krot et al. 1998b, their Fig. 8), and the position of any aqueous to metamorphic boundary was not revealed.

SUMMARY

1. Equilibrium thermodynamic models in multicomponent systems show that fayalite can form during aqueous to metamorphic alteration on parent bodies of ordinary and carbonaceous chondrites. Fayalite can form over a range of temperatures (~30 °C to ~350 °C), pressures, and water/rock ratios (0.06–0.2). Pure fayalite forms at lower temperatures, elevated H$_2$/H$_2$O activity (and/or fugacity) ratios, and higher water/rock ratios.

2. Equilibrium models show that fayalite can form in both metamorphic and aqueous environments. High temperatures (>~200 °C), elevated pressures, the presence of silica phases, and low activities of Mg solutes expand the conditions of fayalite stability and facilitate its aqueous deposition. However, fayalite would never have formed if the alteration occurred at low pressures, which might be typical for highly porous CM and CI carbonaceous chondrites.

3. In equilibrium assemblages, fayalite usually coexists with troilite, magnetite, Ca-Fe pyroxene, kamacite or Ni-rich metal, chromite, phyllosilicates, phosphates, and polyaromatic organic species. At elevated temperatures and pressures, carbides, talc, phlogopite, and amphiboles may also be present. Equilibrium mineralogy is consistent with observations in chondrites.

4. The comparison of models with observations in chondrites reveals that in many cases, fayalite formed during the aqueous to metamorphic transition in sequentially more reducing environments, when the last portions of H$_2$O (liquid and gas) were converted to H$_2$. The mineral most likely was deposited from an aqueous solution with a high activity of H$_2$ and a low activity of water. In subsequent metamorphic reactions, the formation of fayalite then could have continued through the reduction of magnetite by H$_2$ and/or the dehydration of ferrous serpentine. Prolonged and/or high-temperature metamorphism could have then transformed fayalite-bearing assemblages to Ca-Fe pyroxene, Fe-rich metal, and Mg-olivine, leading to the observed absence of fayalite in even moderately metamorphosed chondrites.

5. The low abundances of fayalite in unequilibrated chondrites are likely to be accounted for by the lack of complete equilibration at the narrow range of parameters of fayalite stability in these rocks, consistent with the transient nature of fayalite formation.

Editorial Handling—Dr. Randy Korotev

REFERENCES

Alexander C. M. O'D., Barber D. J., and Hutchison R. 1989. The microstructure of Semarkona and Bishunpur. *Geochimica et Cosmochimica Acta* 53:3045–3057.

Bales R. C. and Morgan J. J. 1985. Dissolution kinetics of chrysotile at pH 7 to 10. *Geochimica et Cosmochimica Acta* 49:2281–2288.

Brearley A. J. 1999. Origin of graphitic carbon and pentlandite in matrix olivines in the Allende meteorite. *Science* 285:1380–1382.

Brearley A. J. and Jones R. H. 1998. Chondritic materials. *Planetary materials,* edited by Papike J. J. Washington, D.C.: Mineralogical Society of America. pp. 3-1–3-398.

Brigham C. A., Yabuki H., Ouyang Z., Murrell M. T., El Goresy A., and Burnett D. S. 1986. Silica-bearing chondrites and clasts in ordinary chondrites. *Geochimica et Cosmochimica Acta* 50: 1655–1666.

Chatterjee N. 1987. Evaluation of thermochemical data on Fe-Mg olivine, orthopyroxene, spinel and Ca-Fe-Mg-Al garnet. *Geochimica et Cosmochimica Acta* 51:2515–2525.

Choi B.-G., Krot A. N., and Wasson J. T. 2000. Oxygen isotopes in magnetite and fayalite in CV chondrites Kaba and Mokoia. *Meteoritics & Planetary Science* 35:1339–1348.

Clayton R. N. and Mayeda T. K. 1999. Oxygen isotope studies of carbonaceous chondrites. *Geochimica et Cosmochimica Acta* 63: 2089–2104.

Deer W. A., Howie R. A., and Zussman J. 1982. *Orthosilicates*. London: Longman. 919 p.

Dodd R. T., van Schmus V. R, and Marvin U. B. 1966. Significance

of iron-rich silicates in the Mezö-Madaras chondrite. *American Mineralogist* 51:1177–1191.

Dove P. M. 1994. The dissolution kinetics of quartz in sodium chloride solutions at 25 °C to 300 °C. *American Journal of Science* 294:665–712.

Ebel D. S. 2006. Condensation of rocky material in astrophysical environments. In *Meteorites and the early solar system II,* edited by Lauretta D. S., McSween H. Y., Jr., and Leshin L. Tucson, Arizona: The University of Arizona Press. pp. 253–277.

Ebel D. S. and Grossman L. 2000. Condensation in dust-enriched systems. *Geochimica et Cosmochimica Acta* 64:339–366.

Fedkin A. V. and Grossman L. 2006. The fayalitic content of chondritic olivine: Obstacle to understanding the condensation of rocky material. In *Meteorites and the early solar system II,* edited by Lauretta D. S., McSween H. Y., Jr., and Leshin L. Tucson, Arizona: The University of Arizona Press. pp. 279–294.

Helgeson H. C., Delany J., and Bird D. K. 1978. Summary and critique of the thermodynamic properties of rock-forming minerals. *American Journal of Science* 278A:1–229.

Hill P. G. 1990. A unified fundamental equation for the thermodynamic properties of H_2O. *Journal of Physical and Chemical Reference Data* 19:1233–1274.

Holland T. J. B. and Powell R. 1998. An internally consistent thermodynamic data set for phases of petrologic interest. *Journal of Metamorphic Geology* 16:309–343.

Holland T. J. B., Baker J., and Powell R. 1998. Mixing properties and activity-composition relationships of chlorites in the system $MgO-FeO-Al_2O_3-H_2O$. *European Journal of Mineralogy* 10: 395–406.

Hua X. and Buseck P. R. 1995. Fayalite in the Kaba and Mokoia carbonaceous chondrites. *Geochimica et Cosmochimica Acta* 59: 563–578.

Hua X., Huss G. R., Tachibana S., and Sharp T. G. 2005. Oxygen, silicon, and Mn-Cr isotopes of fayalite in the Kaba oxidized CV3 chondrite: Constraints for its formation history. *Geochimica et Cosmochimica Acta* 69:1333–1348.

Hutcheon I. D., Krot A. N., Keil K., Phinney D. L., and Scott E. R. D. 1998. ^{53}Mn-^{53}Cr dating of fayalite formation in the CV3 chondrite Mokoia: Evidence for asteroidal alteration. *Science* 282:1865–1867.

Icenhower J. P. and Dove P. M. 2000. The dissolution kinetics of amorphous silica into sodium chloride solutions: Effects of temperature and ionic strength. *Geochimica et Cosmochimica Acta* 64:4193–4203.

Jarosewich E. 1990. Chemical analyses of meteorites: A compilation of stony and iron meteorite analyses. *Meteoritics* 25:323–337.

Jogo K., Nakamura T., and Noguchi T. 2006. Secondary fayalite in the Vigarano CV3 carbonaceous chondrite: Occurrence and formation age (abstract). *Meteoritics & Planetary Science* 41: A88.

Keller L. P. and Buseck P. R. 1990. Aqueous alteration in the Kaba CV3 carbonaceous chondrite. *Geochimica et Cosmochimica Acta* 54:2113–2120.

Keller L. P., Thomas K. L., Clayton R. N., Mayeda T. K., DeHart J. M., and McKay D. S. 1994. Aqueous alteration of the Bali CV3 chondrite: Evidence from mineralogy, mineral chemistry, and oxygen isotopic composition. *Geochimica et Cosmochimica Acta* 58:5589–5598.

Kishima N. and Sakai H. 1984. A simple gas analytical technique for the Dickson-type hydrothermal apparatus and its application to the calibration of MH, NNO, and FMQ oxygen buffers. *Geochemical Journal* 18:19–29.

Kojima T. and Tomeoka K. 1996. Indicators of aqueous alteration and thermal metamorphism on the CV3 parent body: Microstructures of a dark inclusion from Allende. *Geochimica et Cosmochimica Acta* 60:2651–2666.

Komatsu M., Krot A. N., Fagan T., Miyamoto M., Mikouchi T., and Keil K. 2006. Amoeboid olivine aggregates in Yamato-86009 CV chondrite: Evidence for in situ alteration (abstract). *Meteoritics & Planetary Science* 41:A99.

Krot A. N. and Todd C. S. 1998. Metal-carbide-magnetite-fayalite association in a Bali-like clast in the reduced CV3 chondrite breccia Vigarano (abstract). *Meteoritics & Planetary Science* 33: A89.

Krot A. N. and Wasson J. T. 1994. Silica-merrihueite/roedderite-bearing chondrules and clasts in ordinary chondrite: New occurrences and possible origin. *Meteoritics* 29:707–718.

Krot A. N., Scott E. R. D., and Zolensky M. E. 1995. Mineralogical and chemical variations among CV3 chondrites and their components: Nebular and asteroidal processing. *Meteoritics* 30: 748–775.

Krot A. N., Scott E. R. D., and Zolensky M. E. 1997. Origin of fayalitic olivine rims and plate-like matrix olivine in the CV3 chondrite Allende and its dark inclusions. *Meteoritics & Planetary Science* 32:31–49.

Krot A. N., Petaev M. I., Scott E. R. D., Zolensky M. E., Keil K., Scott E. R. D., and Nakamura K. 1998a. Secondary calcium-iron-rich minerals in the Bali-like and Allende-like oxidized CV3 chondrites and Allende dark inclusions. *Meteoritics & Planetary Science* 33:623–645.

Krot A. N., Petaev M. I., Scott E. R. D., Choi B.-G., Zolensky M. E., and Keil K. 1998b. Progressive alteration in CV3 chondrites: More evidence for asteroidal alteration. *Meteoritics & Planetary Science* 33:1065–1085.

Krot A. N., Brearley A. J., Petaev M. I., Kallemeyn G. W., Sears D. W. G., Benoit P. H., Hutcheon I. D., Zolensky M. E., and Keil K. 2000a. Evidence for low-temperature growth of fayalite and hedenbergite in MacAlpine Hills 88107, an ungrouped carbonaceous chondrite related to the CM-CO clan. *Meteoritics & Planetary Science* 35:1365–1386.

Krot A. N., Meibom A., and Keil K. 2000b. A clast of Bali-like oxidized CV material in the reduced CV chondrite breccia Vigarano. *Meteoritics & Planetary Science* 35:817–825.

Krot A. N., Petaev M. I., and Bland P. A. 2004. Multiple formation mechanisms of ferrous olivine in CV carbonaceous chondrites during fluid-assisted metamorphism. *Antarctic Meteorite Research* 17:153–171.

Lauretta D. S. and Buseck P. R. 2003. Opaque minerals in chondrites and fine-grained chondrules rims in the Bishunpur (LL3.1) chondrite. *Meteoritics & Planetary Science* 38:59–79.

Lauretta D. S., Buseck P. R., and Zega T. J. 2001. Opaque minerals in the matrix of the Bishunpur (LL3.1) chondrite: Constraints on the chondrules formation environment. *Geochimica et Cosmochimica Acta* 65:1337–1353.

Lindsley D. H., Grover J. E., and Davidson P. M. 1981. The thermodynamics of the $Mg_2Si_2O_6-CaMgSi_2O_6$ join: A review and a new model. In *Advances in Physical Geochemistry,* vol. 1, edited by Saxena S. K. New York: Springer-Verlag. pp. 149–176.

McSween H. Y., Jr., and Labotka T. C. 1993. Oxidation during metamorphism of the ordinary chondrites. *Geochimica et Cosmochimica Acta* 57:1105–1114.

Mironenko M. V. and Zolotov M. Yu. 2005. Thermodynamic models for aqueous alteration coupled with volume and pressure changes in asteroids (abstract #2207). 36th Lunar and Planetary Science Conference. CD-ROM.

Mironenko M. V., Akinfiev N. N., and Melikhova T. Yu. 2000. GEOCHEQ—The complex for thermodynamic modeling of geochemical systems (abstract). *Herald DGGGMS RAS* 5:96–97.

Ottonello G. 1997. *Principles of geochemistry.* New York: Columbia University Press. 894 p.

Ottonello G., Delta Giusta A., Dal Negro A., and Baccarin F. 1992. A structure-energy model for C2/c pyroxenes in the system Na-

Mg-Ca-Mn-Fe-Al-Cr-Ti-Si-O. In *Advances in physical geochemistry,* edited by Saxena S. K. Berlin: Springer-Verlag. 353 p.

Palme H. and Fegley B. 1990. High-temperature condensation of iron-rich olivine in the solar nebula. *Earth and Planetary Science Letters* 101:180–195.

Peng D. Y. and Robinson D. B. 1976. A new two-constant equation of state. *Industrial and Engineering Chemistry Fundamentals* 15: 59–64.

Petaev M. I. and Mironenko M. V. 1997. Thermodynamic modeling of aqueous alteration in CV chondrites (abstract). Workshop on Parent-Body and Nebular Modification of Chondritic Materials. pp. 49–50.

Powell R. and Holland T. J. B. 1999. Relating formulations of the thermodynamics of mineral solid solutions: Activity modeling of pyroxenes, amphiboles, and micas. *American Mineralogist* 84:1–14.

Rambaldi E. R. and Wasson J. T. 1981. Metal and associated phases in Bishunpur, a highly unequilibrated ordinary chondrite. *Geochimica et Cosmochimica Acta* 45:1001–1015.

Rosenberg N. D., Browning L., and Bourcier W. L. 2001. Modeling of aqueous alteration of CM carbonaceous chondrites. *Meteoritics & Planetary Science* 36:239–244.

Rasmussen, M. G., Evans B. W., and Kuehner S. M. 1998. Low-temperature fayalite, greenalite, and minnesotaite from the Overlook gold deposit, Washington: Phase relations in the system FeO-SiO$_2$-H$_2$O. *Canadian Mineralogist* 36:147–162.

Saxena S. K., Sykes J., and Eriksson G. 1986. Phase equilibria in the pyroxene quadrilateral. *Journal of Petrology* 27:843–852.

Schulte M. and Shock E. 2004. Coupled organic synthesis and mineral alteration on meteorite parent bodies. *Meteoritics & Planetary Science* 39:1577–1590.

Shock E. L., Helgeson H. C., and Sverjensky D. A. 1989. Calculation of the thermodynamic and transport properties of aqueous species at high pressures and temperatures: Standard partial and molar properties of inorganic neutral species. *Geochimica et Cosmochimica Acta* 53:2157–2183.

Shock E. L., Oelkers E. H., Johnson J. W., Sverjensky D. A., and Helgeson H. C. 1992. Calculation of the thermodynamic properties of aqueous species at high pressures and temperatures:

Effective electrostatic radii, dissociation constants, and standard partial molal properties to 1000 °C and 5 kb. *Journal of Chemical Society, Faraday Transactions* 88:803–826.

Shock E. L., Sassani D. C., Willis M., and Sverjensky D. A. 1997. Inorganic species in geologic fluids: Correlations among standard molal thermodynamic properties of aqueous ions and hydroxide complexes. *Geochimica et Cosmochimica Acta* 61: 907–950.

Tacker R. C. and Stormer J. C. 1989. A thermodynamic model for apatite solid solutions, applicable to high-temperature geologic problems. *American Mineralogist* 74:877–888.

Tanger J. C. IV and Helgeson H. C. 1988. Calculation of the thermodynamic and transport properties of aqueous species at high pressures and temperatures: Revised equations of state for standard partial molal properties of ions and electrolytes. *American Journal of Science* 288:19–98.

Van Zeggeren F. and Storey S. H. 1970. *The computation of chemical equilibria.* Cambridge: Cambridge University Press. 176 p.

Wasson J. and Krot A. N. 1994. Fayalite-silica association in unequilibrated ordinary chondrites: Evidence for aqueous alteration on a parent body. *Earth and Planetary Science Letters* 122: 403–416.

Wilson L., Keil K., Browning L. B., Krot A. N., and Bourcier W. 1999. Early aqueous alteration, explosive disruption, and re-processing of asteroids. *Meteoritics & Planetary Science* 34: 541–557.

Weisberg M. K. and Prinz M. 1998. Fayalitic olivine in CV3 chondrite matrix and dark inclusions: A nebular origin. *Meteoritics & Planetary Science* 33:1087–1099.

Weisberg M. K., Zolensky M. E., and Prinz M. 1997. Fayalite olivine in matrix of the Krymka LL3.1 chondrite: Vapor-solid growth in the solar nebula. *Meteoritics & Planetary Science* 32: 791–801.

Wood J. A. and Holmberg B. B. 1994. Constraints placed on chondrules-forming process by merrihueite in the Mezö-Madaras chondrite. *Icarus* 108:309–324.

Zolensky M. E., Bourcier W. L. and J. L. Gooding 1989. Aqueous alteration on the hydrous asteroids: Results of EQ3/6 computer simulations. *Icarus* 78:411–425.

APPENDIX

Table A1. The components of solid solutions and Margules parameters of mixing.

Solid solution	End members	W_H (cal/mole)	W_S (cal/mole/K)	W_V (cal/bar/mole)	Reference
Fe-Mg olivine	Forsterite, Mg$_2$SiO$_4$	2151	0	0	Chatterjee 1987
	Fayalite, Fe$_2$SiO$_4$	2151	0	0	
Mg-Fe orthopyroxene	Enstatite, Mg$_2$Si$_2$O$_6$	3131	3.585	0	Ottonello et al. 1992
	Ferrosilite, Fe$_2$Si$_2$O$_6$	805.5	1.195	0	
Mg$_2$-CaMg orthopyroxene	Enstatite, Mg$_2$Si$_2$O$_6$	5975	0	0	Lindsley et al. 1981
	Orthodiopside, CaMgSi$_2$O$_6$	5975	0	0	
Mg$_2$-CaFe orthopyroxene	Enstatite, Mg$_2$Si$_2$O$_6$	14.34	0	0	Lindsley et al. 1981
	Orthohedenbergite, CaFeSi$_2$O$_6$	7.17	0	0	
Fe$_2$-CaMg orthopyroxene	Orthoferrosilite, Fe$_2$Si$_2$O$_6$	3824	0	0	Saxena et al. 1986
	Orthodiopside, CaMgSi$_2$O$_6$	4780	0	0	
Fe$_2$-CaFe orthopyroxene	Ferrosilite, Fe$_2$Si$_2$O$_6$	7170	0	0	Lindsley et al. 1981
	Orthohedenbergite, CaFeSi$_2$O$_6$	7887	0	0	
CaMg-CaFe orthopyroxene	Orthodiopside, CaMgSi$_2$O$_6$	1195	0	0	Saxena et al. 1986
	Orthohedenbergite, CaFeSi$_2$O$_6$	1673	0	0	
Mg-Fe clinopyroxene	Clinoenstatite, Mg$_2$Si$_2$O$_6$	−372.5	5.829	0.0067	Ottonello et al. 1992
	Clinoferrosilite, Fe$_2$Si$_2$O$_6$	602.0	5.891	0.0054	

Table A1. *Continued.* The components of solid solutions and Margules parameters of mixing.

Solid solution	End members	W_H (cal/mole)	W_S (cal/mole/K)	W_V (cal/bar/mole)	Reference
Mg$_2$-CaMg clinopyroxene	Clinoenstatite, Mg$_2$Si$_2$O$_6$	6091	0	0.0194	Lindsley et al. 1981
	Clinodiopside, CaMgSi$_2$O$_6$	7461	0	−0.0015	
Mg$_2$-CaFe clinopyroxene	Clinoenstatite, Mg$_2$Si$_2$O$_6$	22,299	10.75	0	Saxena et al. 1986
	Clinohedenbergite, CaFeSi$_2$O$_6$	4780	−6.69	0	
Fe$_2$-CaMg clinopyroxene	Clinoferrosilite, Fe$_2$Si$_2$O$_6$	3585	0	0	Saxena et al. 1986
	Clinodiopside, CaMgSi$_2$O$_6$	5736	0	0	
Fe$_2$-CaFe clinopyroxene	Clinoferrosilite, Fe$_2$Si$_2$O$_6$	4049	0	0.0014	Lindsley et al. 1981
	Clinohedenbergite, CaFeSi$_2$O$_6$	4947	0	−0.0055	
CaMg-CaFe clinopyroxene	Clinodiopside, CaMgSi$_2$O$_6$	2868	0	0	Saxena et al. 1986
	Clinohedenbergite, CaFeSi$_2$O$_6$	2868	0	0	
Fe-Mg chlorite	Daphnite, Fe$_5$Al$_2$Si$_3$O$_{10}$(OH)$_8$	597.5	0	0	Holland et al. 1998
	Clinochlore, Mg$_5$Al$_2$Si$_3$O$_{10}$(OH)$_8$	597.5	0	0	
Phlogopite-annite	Phlogopite, KMg$_3$[AlSi$_3$O$_{10}$](OH)$_2$	2151	0	0	Powell and Holland 1999
	Annite, KFe$_3$[AlSi$_3$O$_{10}$](OH)$_2$	2151			
Mg-Fe talc	Talc, Mg$_3$Si$_4$O$_{10}$(OH)$_2$	0	0	0	Holland and Powell 1998
	Fe talc, Fe$_3$Si$_4$O$_{10}$(OH)$_2$	0	0	0	
OH-Cl apatite	Hydroxylapatite, Ca$_5$(PO$_4$)$_3$(OH)	−4780	0	0	Tacker and Stormer 1989
	Chlorapatite, Ca$_5$(PO$_4$)$_3$Cl	−4780	0	0	
Tremolite-ferroactinolite	Tremolite, Ca$_2$Mg$_5$Si$_8$O$_{22}$(OH)$_2$	0	0	0	
	Ferroactinolite, Ca$_2$Fe$_5$Si$_8$O$_{22}$(OH)$_2$	0	0	0	
Fe-Ni-Co-Cr metal alloy	Fe^0 metal	0	0	0	
	Ni^0 metal	0	0	0	
	Co^0 metal	0	0	0	
	Cr^0 metal	0	0	0	
Chrysotile-greenalite	Chrysotile, Mg$_3$Si$_2$O$_5$(OH)$_4$	0	0	0	
	Greenalite, Fe$_3$Si$_2$O$_5$(OH)$_4$	0	0	0	
Na-K-Mg-Ca saponite	Na saponite, Na$_2$Mg$_{18}$Al$_2$[Si$_{22}$O$_{60}$](OH)$_{12}$	0	0	0	
	K saponite, K$_2$Mg$_{18}$Al$_2$[Si$_{22}$O$_{60}$](OH)$_{12}$	0	0	0	
	Mg saponite, MgMg$_{18}$Al$_2$[Si$_{22}$O$_{60}$](OH)$_{12}$	0	0	0	
	Ca saponite, CaMg$_{18}$Al$_2$[Si$_{22}$O$_{60}$](OH)$_{12}$	0	0	0	

Margules parameters are calculated with the equation $W_{ij} = WH_{ij} - T \cdot WS_{ij} + P \cdot WV_{ij}$, where T designates absolute temperature and P stands for pressure. Activity coefficients (γ_i) of components in solid solutions are calculated with the subregular binary model with equations $\ln(\gamma_1) = X_2^2[W_{12} + 2X_1(W_{21} - W_{12})]/RT$ and $\ln(\gamma_2) = X_1^2[W_{21} + 2X_2^2(W_{12} - W_{21})]/RT$, where X_i represent mole fraction of a component in solution and R stands for the universal gas constant.

Table A2. Molar amounts of chemical elements per 1 kg of chondrites.

Chondrite	O	H	K	Mg	Ca	Al	C	Si	P	S	Cr	Na	Cl	Mn	Fe	Co	Ni
Sharps, H3	19.4713	0.5257	0.0158	5.8718	0.3245	0.3965	0.8416	6.2675	0.0435	0.6984	0.0614	0.2815	0.00420	0.0450	5.0086	0.0162	0.3082
Mezö-Madaras, L3	21.3175	0.2501	0.0244	6.3877	0.3749	0.3980	0.4006	6.8911	0.0398	0.7151	0.0697	0.3342	0.00590	0.0575	4.0454	0.0106	0.2210
Krymka, LL3	22.1855	0.1623	0.0206	6.5988	0.3589	0.4644	0.2599	7.1920	0.0334	0.7321	0.0773	0.2813	0.00607	0.0501	3.6303	0.0091	0.1779
Bishunpur, LL3	21.8510	0.2889	0.0222	6.5149	0.3419	0.4583	0.4623	7.0694	0.0443	0.7711	0.0685	0.3212	0.00591	0.0473	3.7469	0.0107	0.1874
Semarkona, LL3	22.0632	0.3169	0.0226	6.5688	0.3874	0.4658	0.5054	7.1179	0.0360	0.6444	0.0669	0.3299	0.00601	0.0525	3.6395	0.0090	0.2105
ALHA77307, CO	19.5959	0.4848	0.0074	6.1774	0.3738	0.5710	0.7756	6.0798	0.0361	0.8239	0.0717	0.0564	0.00920	0.0328	4.8292	0.0119	0.3412
Allende, CV3$_{oxA}$	20.7015	0.1644	0.0069	6.6548	0.5070	0.6987	0.2630	6.2063	0.0353	0.4994	0.0726	0.1582	0.00768	0.0276	4.6491	0.0019	0.0668
Allende (matrix)	19.4146	0.2045	0.0070	5.8012	0.5197	0.6573	0.3271	6.0150	0.0384	0.6816	0.0770	0.1550	0.00770	0.0338	5.2688	0.0037	0.1581
Bali, CV3$_{oxB}$	20.6951	0.3263	0.0140	6.6978	0.5139	0.6818	0.5220	6.1825	0.0403	0.5080	0.0663	0.1846	0.00776	0.0295	4.5962	0.0019	0.0412
Murchison, CM2	19.0951	1.1753	0.0104	6.0429	0.4116	0.5151	1.8812	5.9094	0.0396	1.0058	0.0752	0.0946	0.01480	0.0344	4.8405	0.0104	0.2414

The compositions are calculated on the H$_2$O-free basis from Jarosewich (1990). Note that fayalite has not been detected in the Semarkona, Allende, ALHA77307, and Murchison chondrites.